18. SITE 730[1]

Shipboard Scientific Party[2]

HOLE 730A

Date occupied: 29 September 1987

Date departed: 30 September 1987

Time on hole: 1 day, 10 hr, 45 min

Position: 17°43.885′N, 57°41.519′E

Water depth (sea level; corrected m, echo-sounding): 1065.8

Water depth (rig floor; corrected m, echo-sounding): 1076.3

Bottom felt (m, drill pipe): 1071.4

Penetration (m): 403.9

Number of cores: 42

Total length of cored section (m): 403.9

Total core recovered (m): 323.66

Core recovery (%): 80

Oldest sediment cored:
Depth sub-bottom (m): 403.9
Nature: Foraminifer nannofossil chalk
Age: late early Miocene (NN4)
Measured velocity (km/s): 2.03–2.06

Principal results: Site 730 is situated on the Oman continental margin near the bottom of the pronounced oxygen-minimum zone (OMZ) that impinges on the margin. The age of sediments and hiatuses, and the evolution of the sediment facies, were expected to be useful in reconstructing the subsidence as well as the erosional and tectonic history of the slope basins and the prominent basement ridges.

Some major findings at Site 730 include the identification of

1. a significant hiatus ranging in age from Pleistocene to upper Miocene;
2. the occurrence of siliceous sediments in the middle and upper Miocene that appear earlier here but are generally equivalent to the siliceous facies recovered on the Owen Ridge;
3. the appearance of *Globerigina bulloides,* an upwelling indicator, in the lower middle Miocene, which is earlier than its appearance on the Owen Ridge; and
4. the presence of slumps, faults, and turbidites in the middle Miocene that indicate tectonic instability of the marginal slope basins.

The sediments at Site 730 range from the Holocene to the late early Miocene in age and include one prominent hiatus. Opal deposition and upwelling began earlier on the Oman margin than it did on the offshore Owen Ridge. Site 730 also provided information about the tectonic stability and uplift history of the slope basins and their associated basement ridges.

BACKGROUND AND OBJECTIVES

Site 730 is located at 17°43.885′N and 57°41.519′E in a water depth of 1065.8 m and was the last site drilled on the Oman continental margin. It was selected during operations on Leg 117 and added to the operations schedule after Site 729 was abandoned due to hole conditions. Similar to previous Sites 723 and 727, Site 730 is located near the bottom of the pronounced OMZ that impinges on the margin (Fig. 1).

Site 730 is positioned to the east of a ridge that is presumably ophiolitic basement and separates the upper and lower slope sedimentary basins. The location of Site 730 is shown in Figures 2A and 2B, and its structural and depositional setting is shown in Figures 3A and 3B. The seismic reflection profiles (Figs. 3A and 3B) show that the sediments of the upper basin, which were previously drilled only 6 km to the west at Site 727, onlap eastward onto the ridge and are thinned and tilted by tectonic movement of the ridge. East of the basement ridge, the profiles reveal a prominent unconformity (at about 0.05 s) that truncates eastward-dipping reflectors that extend from about 0.5 to 0.20 s. The eastward-dipping reflectors extend downsection through a zone of relatively diffuse reflections (0.2–0.3 sbsf) to a thick zone of discontinuous dipping reflectors with variable amplitude from 0.3 to about 0.8 sbsf.

The eastward-dipping sediments are truncated to the east by a series of high-angle faults that form a series of steps extending down to the basin where Site 728 is located. These sediments are interpreted as the faulted and tilted remnants of a former slope basin. We moved upsection on the eastward-dipping reflectors and cored through the upper unconformity to recover older slope basin sediments. The ages of the sediments and the hiatus and the evolution of the sediment facies were expected to be useful in reconstructing the subsidence as well as the erosional and tectonic history of the slope basins and the prominent basement ridges.

Specific objectives for drilling at Site 730 were

1. to obtain a high-resolution record of older slope basin sediments that are associated with the proximal zone of the monsoonal upwelling system in order to establish long-term changes in monsoonal timing and intensity;
2. to provide another deep-water component of a depth transect that will be used to examine the organic-rich sedimentary facies of the margin and to establish their diagenetic history and relationship to the OMZ and its spatial variation through time; and
3. to provide constraints on the uplift and erosional history of the basement ridges and their intervening slope basins.

OPERATIONS

After the Science Operator gave us permission to drill a new site (Site 730), *JOIDES Resolution* left Site 729 at 2230 on 28 September 1987 and headed west to Site 730 with the seismic gear deployed. After a survey of 22 nmi, we located the site and dropped the beacon at 0545 hr on 22 September. By 0630 the mud line of Hole 730A was shot in water depths of 1065.8 m. According to the global positioning system (GPS), Site 730 is located at 17°43.885′N and 57°41.519′E; furthermore, we drilled only one hole here.

We recovered 104% of the cored interval with the advanced hydraulic piston corer (APC) system in Cores 117-730A-1H to

[1] Prell, W. L., Niitsuma, N., et al., 1989. *Proc. ODP, Init. Repts.*, 117: College Station, TX (Ocean Drilling Program).

[2] Shipboard Scientific Party is as given in the list of Participants preceding the contents.

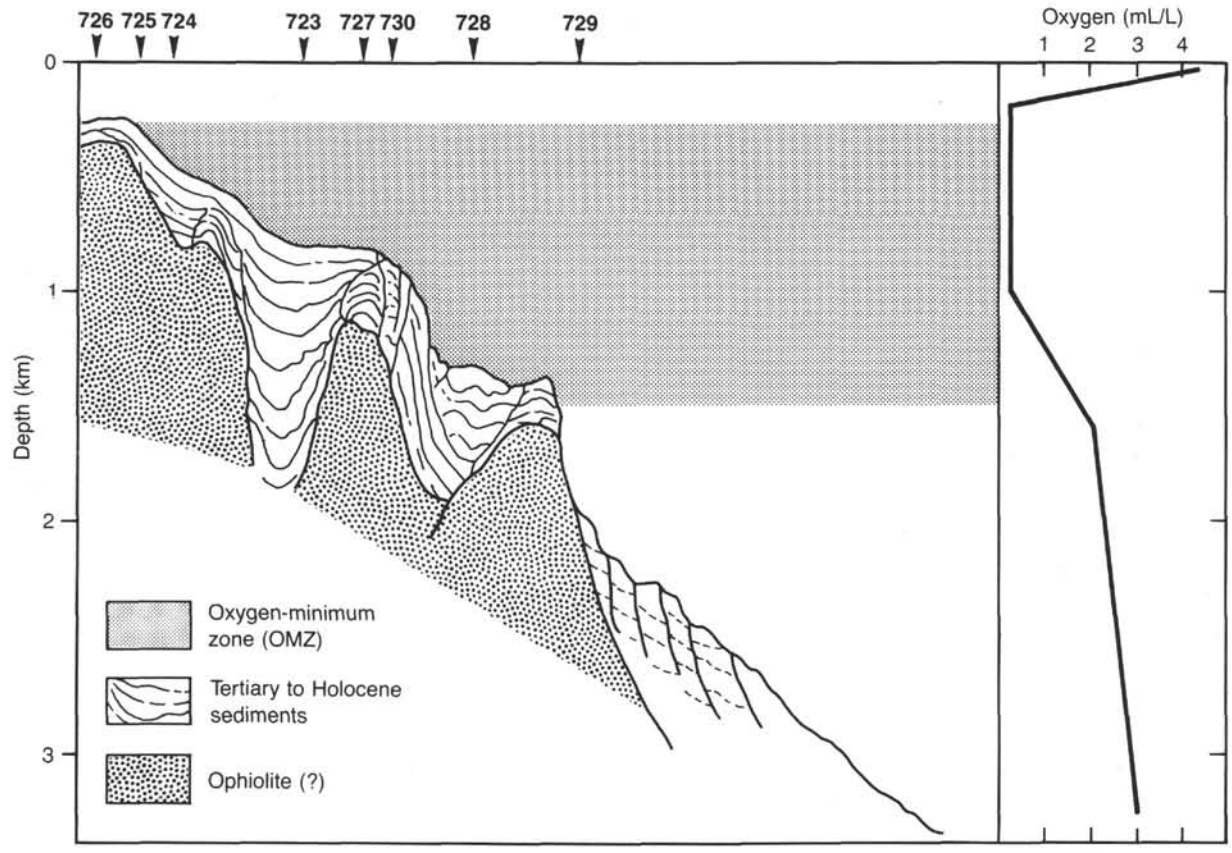

Figure 1. Structure of the Oman margin and the oxygen-minimum zone (OMZ). The schematic profile shows the series of basement ophiolite blocks and the sedimentary basins between them. The concentration of oxygen in the water column (RC2704, unpubl. data) defines the depth range of the OMZ and where it impinges on the margin.

-5H (0–46.3 mbsf). During retrieval of Core 117-730A-5H, a maximum overpull of 60,000 pounds was registered, and we switched the coring mode to the extended core barrel (XCB) system. The total depth of Hole 730A was reached at 403.9 mbsf, when the core barrel parted upon retrieval of Core 117-730A-43X. Recovery with the XCB in the interval from 46.3 to 403.9 mbsf was 75%, which gives an average recovery rate of 80% at Site 730 (Table 1). The long-standing recovery record of 3,841 m, established during Leg 108, was broken with a core recovery of 3,920.2 m during operations on Site 730.

The hole was displaced with heavy mud, and the ship was under way to Site 731 by 1630 hr on 30 September 1987.

LITHOSTRATIGRAPHY

Lithology

The sediments recovered at Site 730 are subdivided into three lithologic units (Fig. 4). Unit I is composed of a relatively thin interval of marly calcareous ooze of Quaternary age, and Unit II is composed of a diatom-bearing sequence of diatomaceous marly nannofossil ooze and diatomaceous silty clays that are late Miocene to middle Miocene age. Unit III, on the other hand, represents calcareous marly chalks and chalks which contain a significant amount of slump horizons and calcareous turbidites. Unit III comprises a lower Miocene to middle Miocene sequence. Table 2 lists the carbonate and organic carbon percentages determined for Site 730; Figure 5 shows the carbonate content of Site 730 sediments.

Unit I (Depth: 0–15.2 mbsf; Age: Holocene to Pleistocene)

Core 117-730A-1H through Section 117A-730A-2H-5, 90 cm.

Unit I is composed of marly to muddy nannofossil-foraminifer ooze and is terminated by an unconformity at 15.2 mbsf. The sediment is olive (5Y 4/3) to olive gray (5Y 5/2) in color and contains 20%–45% foraminifers and 15%–30% nannofossils. Fragments of bivalves and a solitary coral (Fig. 6) were found in this sequence. Authigenic dolomite rhombs occur in proportions of 1%–3%. The lower boundary of this sequence appears as a relatively dark-colored, 50-cm-thick, muddy and bioturbated layer. Sediment from this layer was found within burrows in a 60-cm-thick zone below this horizon (Fig. 7). Also, a single vertical burrow filled with the sediment of Unit I that was 2.25 m long and had a diameter of 2 cm appeared on the split face. Between 2 and 7 m above this major boundary, three horizons approximately 15 cm thick of predominantly vertical burrows were noted. These zones may represent minor hiatuses.

Unit II (Depth: 15.2–201.0 mbsf; Age: middle to late Miocene)

Sections 117-730A-2H-5, 90 cm, through 117-730A-21X, CC.

Unit II is composed of alternating relatively carbonate-rich and carbonate-poor layers which display 0.5–2-m-thick pairs of light and dark layers. Unit II is subdivided into three subunits, based on the presence of diatoms, the differences in carbonate

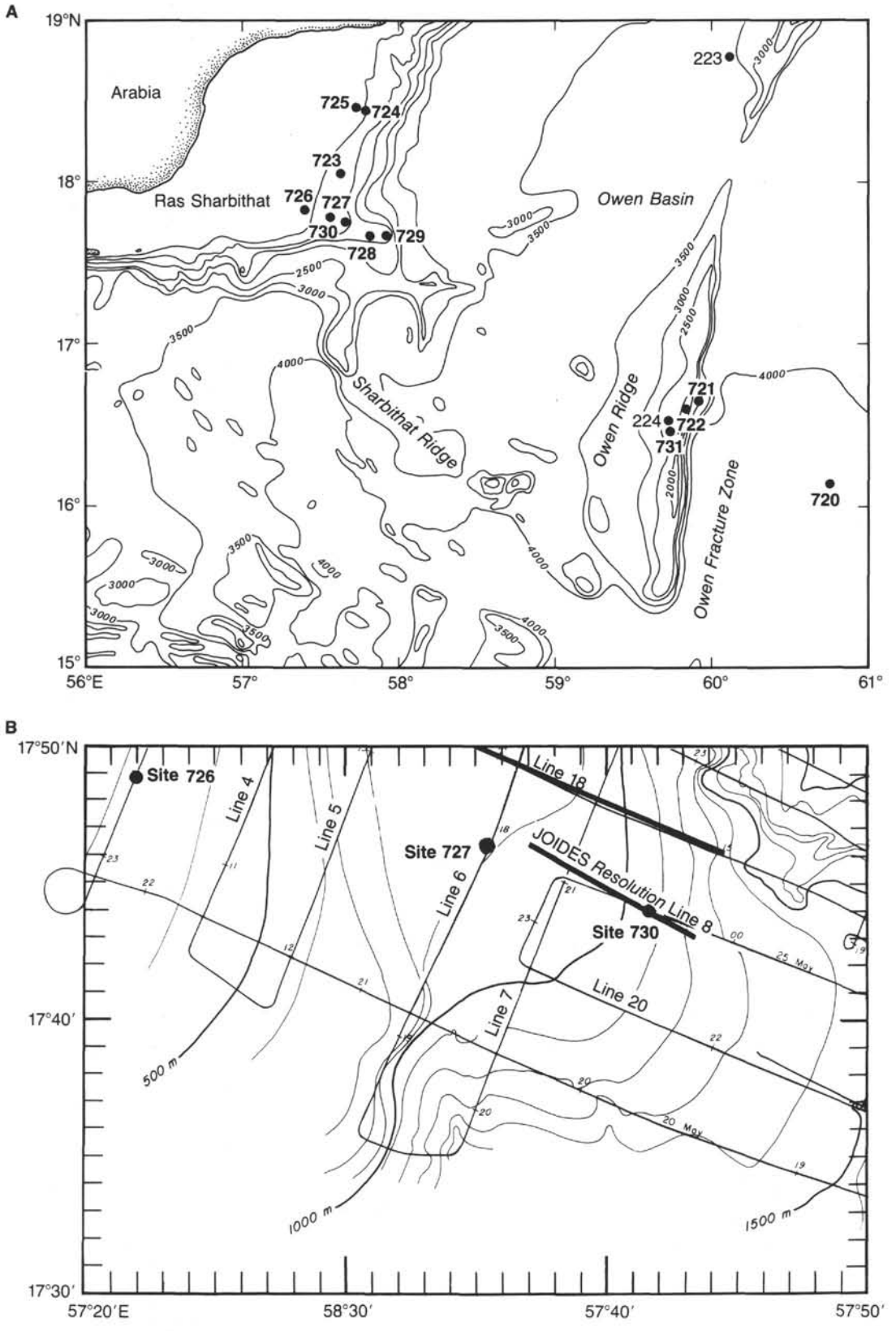

Figure 2. **A.** Bathymetry of the Oman margin and the location of Site 730. **B.** Detailed location of Site 730 and the seismic profiles shown in Figure 3. Bathymetry data are from the site survey (RC2704, 1986).

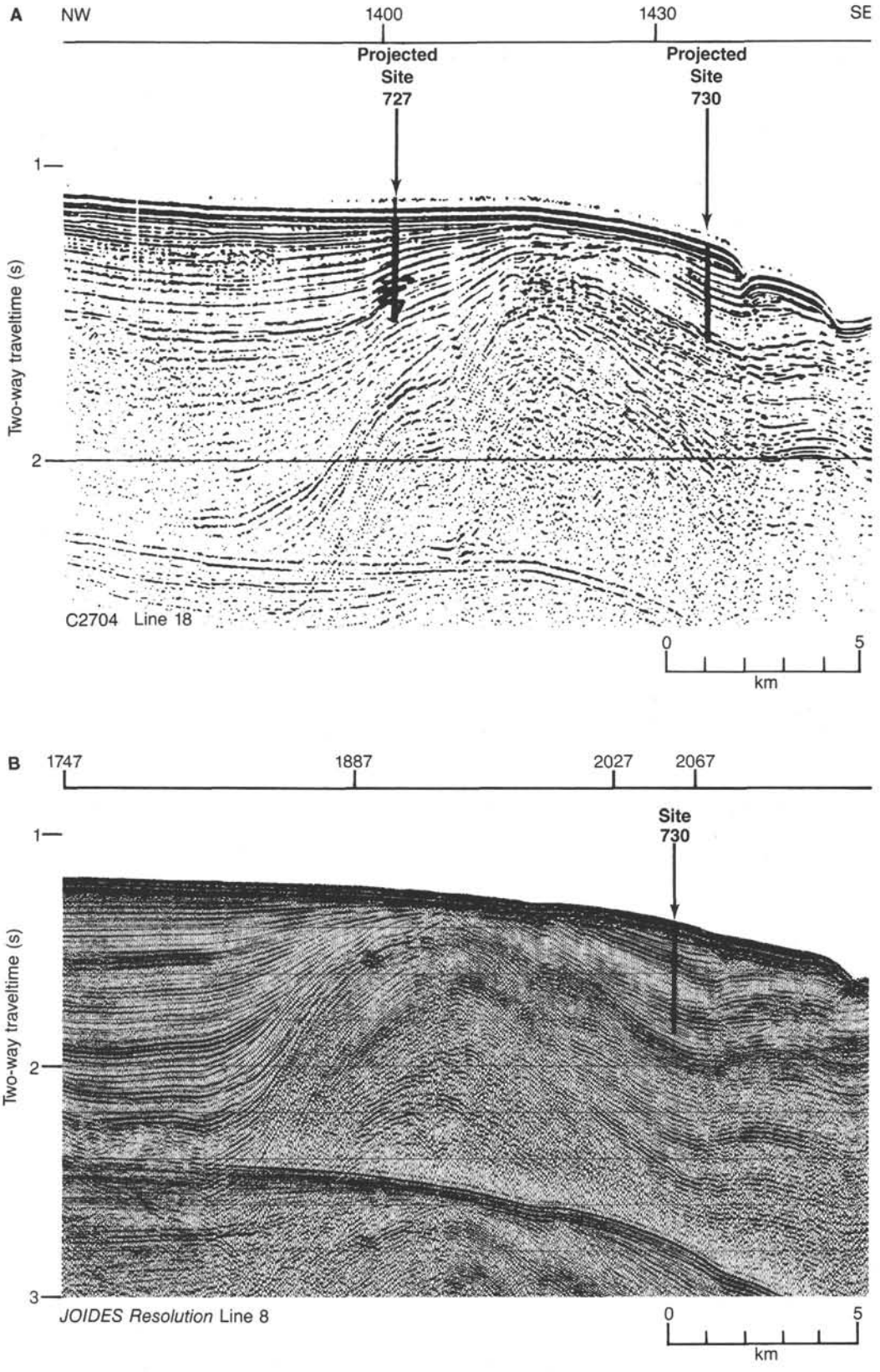

Figure 3. Single channel seismic (SCS) reflection profiles showing the structural and depositional setting of Site 730. A. RC2704 Line 8. B. *JOIDES Resolution* Line 18. Both profiles are perpendicular to the trend of the basin and show the bounding basement blocks and the dipping and truncated slope basin sediments.

Table 1. Coring summary, Site 730.

Core no.	Date (Sept. 1987)	Time (local)	Depth (mbsf)	Cored (m)	Recovered (m)	Recovery (%)
1H	29	1045	0–8.3	8.3	8.32	100.0
2H	29	1100	8.3–17.8	9.5	9.94	104.0
3H	29	1130	17.8–27.3	9.5	9.99	105.0
4H	29	1200	27.3–36.8	9.5	9.97	105.0
5H	29	1230	36.8–46.3	9.5	10.07	106.0
6X	29	1300	46.3–55.8	9.5	9.52	100.0
7X	29	1325	55.8–65.5	9.7	9.53	98.2
8X	29	1344	65.5–75.2	9.7	9.41	97.0
9X	29	1405	75.2–84.9	9.7	9.87	102.0
10X	29	1425	84.9–94.6	9.7	9.44	97.3
11X	29	1445	94.6–104.2	9.6	9.34	97.3
12X	29	1505	104.2–113.9	9.7	9.34	96.3
13X	29	1520	113.9–123.5	9.6	8.03	83.6
14X	29	1540	123.5–133.2	9.7	9.79	101.0
15X	29	1600	133.2–142.9	9.7	9.58	98.7
16X	29	1620	142.9–152.6	9.7	9.62	99.2
17X	29	1640	152.6–162.2	9.6	9.16	95.4
18X	29	1705	162.2–171.9	9.7	9.40	96.9
19X	29	1740	171.9–181.6	9.7	9.47	97.6
20X	29	1805	181.6–191.2	9.6	9.01	93.8
21X	29	1835	191.2–200.9	9.7	9.86	101.0
22X	29	1905	200.9–210.6	9.7	9.81	101.0
23X	29	1930	210.6–220.2	9.6	9.96	104.0
24X	29	1950	220.2–229.9	9.7	9.85	101.0
25X	29	2015	229.9–239.6	9.7	9.49	97.8
26X	29	2040	239.6–249.2	9.6	7.25	75.5
27X	29	2105	249.2–258.9	9.7	6.24	64.3
28X	29	2150	258.9–268.6	9.7	5.71	58.8
29X	29	2220	268.6–278.2	9.6	7.03	73.2
30X	29	2245	278.2–287.9	9.7	8.78	90.5
31X	29	2305	287.9–297.6	9.7	9.54	98.3
32X	29	2330	297.6–307.2	9.6	1.14	11.9
33X	30	0005	307.2–316.9	9.7	6.70	69.1
34X	30	0045	316.9–326.6	9.7	2.34	24.1
35X	30	0130	326.6–336.2	9.6	1.99	20.7
36X	30	0215	336.2–345.9	9.7	1.02	10.5
37X	30	0335	345.9–355.6	9.7	4.72	48.6
38X	30	0430	355.6–365.2	9.6	2.63	27.4
39X	30	0540	365.2–374.9	9.7	3.49	36.0
40X	30	0720	374.9–384.6	9.7	9.79	101.0
41X	30	0915	384.6–394.2	9.6	1.93	20.1
42X	30	1040	394.2–403.9	9.7	5.59	57.6
				403.9	323.66	

and organic carbon content, and distinctions in trace fossil assemblages.

Subunit IIA (Depth: 15.2–33.2 mbsf)

Subunit IIA is composed of distinct alternations between carbonate-rich and carbonate-poor layers with pairs of light and dark layers about 60 cm thick. These sediments are olive (5Y 4/3) to dark olive (5Y 3/3) in color. Bioturbation mottling is abundant throughout this subunit and includes traces of *Zoophycus*. The carbonate content ranges from 30% to 40%, and organic carbon displays values from 1% to 1.5%.

Subunit IIB (Depth: 33.2–150.45 mbsf)

Subunit IIB is a dominantly carbonate-poor (Fig. 5), diatomaceous marly nannofossil ooze with alternating carbonate-rich and carbonate-poor layers that have an organic carbon content from 2% to 4% (Table 2). Colors range from olive gray (5Y 5/2) to olive (5Y 4/3) in the light layers and dark olive gray (5Y 3/2) in the dark layers.

Evidence of bioturbation is seen throughout Subunit IIB. Bioturbation displays the typical infill pattern of dark-colored sediment into the top of the light layers and of light-colored sediment into the top of the dark layers. Some of the dark-colored

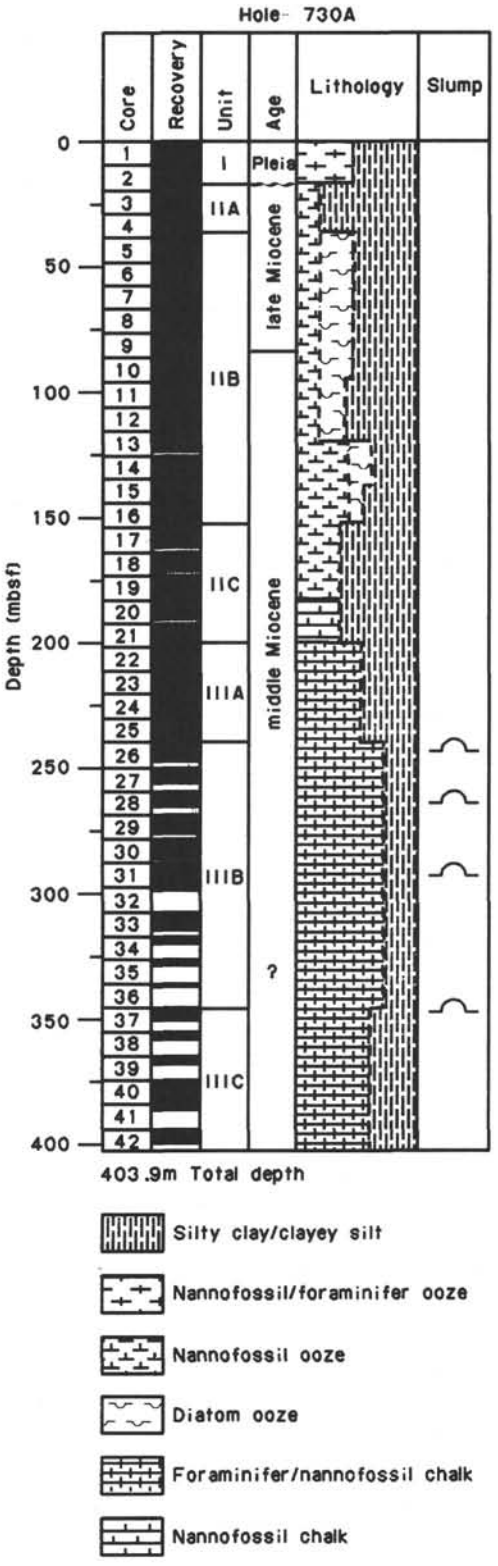

Figure 4. Lithologic summary of Site 730. ⌒ = slump horizons.

layers seem to have a slightly lesser degree of bioturbation when compared with the light-colored ones. Among the trace fossils observed are *Planolites, Teichichnus,* and *Chondrites*, whereas *Zoophycus* is relatively rare. The diatom content ranges between 10% and 40% (Fig. 8) and shows two major patterns in its distribution. On a large scale, the highest diatom content and the

Table 2. Calcium carbonate and organic carbon contents, Site 730.

Core, section, interval (cm)	Depth (mbsf)	Total carbon (%)	Inorganic carbon (%)	Organic carbon (%)	$CaCO_3$ (%)
117-730A-					
1H-3, 78–80	3.78	8.75	7.47	1.28	62.2
2H-2, 78–80	10.58	9.73	8.81	0.92	73.4
3H-2, 130–132	20.60	5.88	4.27	1.61	35.6
4H-2, 78–80	29.58	7.07	5.56	1.51	46.3
5H-2, 80–82	39.10	4.88	2.89	1.99	24.1
6X-2, 105–107	48.85	5.47	2.08	3.39	17.3
7X-1, 130–132	57.10	5.21	2.33	2.88	19.4
8X-2, 109–111	68.09	4.27	2.18	2.09	18.2
9X-2, 78–80	77.48	4.98	2.35	2.63	19.6
10X-2, 78–80	87.18	8.28	6.40	1.88	53.3
11X-2, 110–112	97.20	6.78	3.68	3.10	30.7
12X-2, 78–80	106.48	8.83	4.79	4.04	39.9
13X-2, 128–130	116.68	7.69	5.93	1.76	49.4
14X-2, 78–80	125.78	8.42	8.04	0.38	67.0
15X-2, 30–32	135.00	9.24	8.42	0.82	70.1
16X-2, 14–16	144.54	7.69	6.78	0.91	56.5
17X-2, 73–75	154.83	6.14	4.99	1.15	41.6
18X-2, 36–38	164.06	7.07	6.14	0.93	51.2
19X-2, 60–62	174.00	9.39	9.35	0.04	77.9
20X-2, 93–95	184.03	8.31	7.54	0.77	62.8
21X-2, 78–80	193.48	6.87	6.01	0.86	50.1
22X-2, 123–125	203.63	6.46	5.48	0.98	45.7
23X-2, 88–90	212.98	6.64	6.00	0.64	50.0
24X-2, 71–73	222.41	7.62	7.27	0.35	60.6
25X-2, 87–89	232.27	7.55	6.94	0.61	57.8
26X-4, 72–74	244.82	10.50	10.36	0.14	86.3
27X-4, 91–93	254.61	9.89	9.79	0.10	81.6
28X-4, 80–82	264.20	9.32	9.00	0.32	75.0
29X-3, 65–67	272.25	11.25	11.19	0.06	93.2
29X-5, 70–72	275.30	6.58	6.21	0.37	51.7
30X-6, 59–61	286.29	8.64	8.46	0.18	70.5
31X-1, 87–90	288.77	6.79	6.38	0.41	53.2
32X-1, 48–50	298.08	11.26	11.21	0.05	93.4
33X-1, 29–31	307.49	10.91	10.86	0.05	90.5
34X-1, 50–52	317.40	11.67	11.30	0.37	94.1
35X-1, 17–19	326.77	11.43	11.30	0.13	94.1
37X-1, 81–83	346.71	10.55	10.36	0.19	86.3
38X-2, 21–23	357.31	7.63	7.36	0.27	61.3
39X-1, 75–77	365.95	10.75	10.70	0.05	89.1
40X-2, 20–22	376.60	9.07	9.02	0.05	75.1
41X-1, 54–56	385.14	5.58	5.48	0.10	45.7
42X-1, 97–99	395.17	10.55	10.53	0.02	87.7

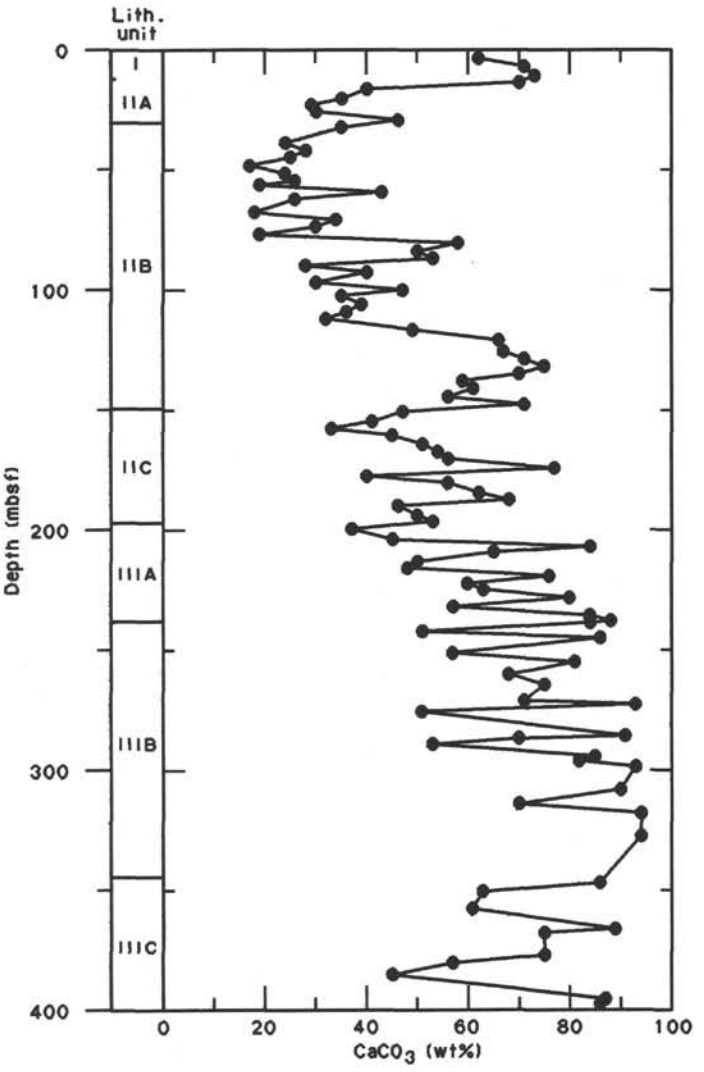

Figure 5. Carbonate contents of Hole 730A.

lowest carbonate content (Fig. 5) are observed in the upper part of Subunit IIB. On a scale of beds, dark layers are richer in diatoms and poorer in nannofossils compared with the lighter, carbonate-rich layers (Fig. 8). The difference in carbonate content between most light and dark layers is 10%–15%.

The lower interval of Subunit IIB (Sections 117-730A-13X-5, 20 cm, to 117-730A-16X-6; 120.1–150.5 mbsf) has a relatively high carbonate content (55%–75%; Fig. 5) with 5%–15% diatoms (Fig. 8). Sediment colors range from light gray (5Y 7/2) to light olive gray (5Y 6/2) to olive gray (5Y 5/2) to olive (5Y 4/3). The sediments display well-developed light and dark alterations which have an average thickness of 1.5 m. Mottling by bioturbation is well developed, and organic carbon values are relatively low (~1%).

Subunit IIC (Depth: 150.45–201.0 mbsf)

Subunit IIC shows a well-developed to indistinctly developed light-dark alternation on the scale of 1–1.5 m. Sediment colors range from light olive gray (5Y 6/2) to olive gray (5Y 5/2) to olive (5Y 5/3). Subunit IIC is composed of 35%–80% carbonate (with a mean of roughly 50%) and less than 5% foraminifers. Less than 2% of the components are diatoms, which distinguishes this subunit from the diatomaceous Subunit IIB. Bio-

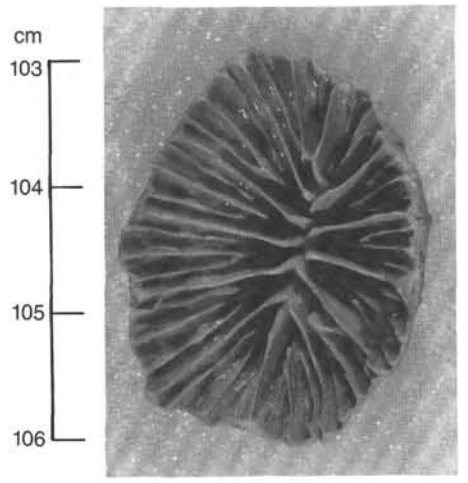

Figure 6. Solitary coral in Unit I (Section 117-730A-2H-1, 103–106 cm).

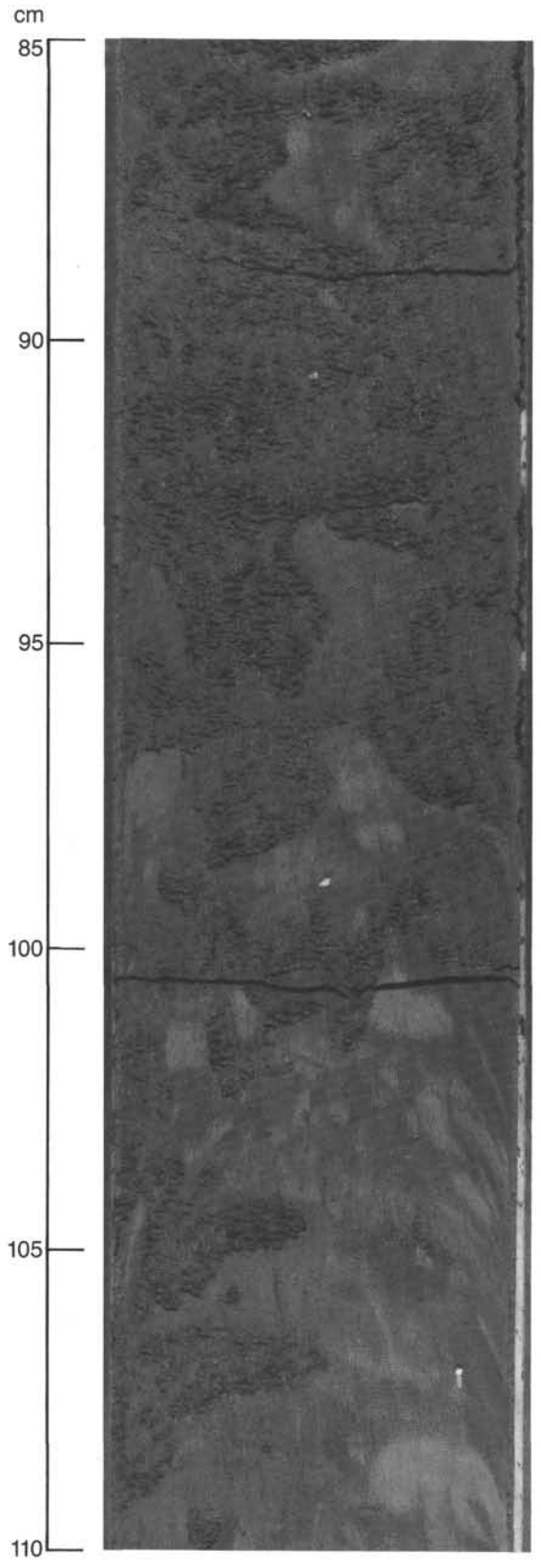

Figure 7. Bioturbated contact defining the unconformity between Units I and II (Section 117-730A-2H-5, 85–110 cm).

turbation and trace fossils are the same as described in Subunit IIB. The ooze-chalk transition occurs at roughly 180 mbsf. The first set of subvertical joints and features of other small offsets are found in Core 117-730A-20X (184.5 mbsf).

Unit III (Depth: 201.0–403.9 mbsf; Age: middle Miocene to early Miocene)

Sections 117-730A-21X, CC, through 117-730A-42X, CC

Unit III is composed of chalk with relatively high carbonate and foraminifer contents. It is subdivided into three subunits that are composed of two pelagic chalk sequences separated by a chalk layer that contains slump deposits and calcareous turbidites.

Subunit IIIA (Depth: 201.0–239.6 mbsf)

Subunit IIIA is comprised of foraminifer-rich marly chalk to chalk. Carbonate contents range from 50% to 90% (Fig. 5). The sequence displays a well-developed light-dark alternation spaced 0.9–1.5 m apart. Colors vary from light gray (5Y 7/2) to light olive gray (5Y 6/2) to olive gray (5Y 5/2) and are related to fluctuations in the carbonate content. Light-colored layers have a higher foraminifer (30%) and nannofossil (~70%) content and a lower amount of detrital calcite (roughly 5%) compared with the dark layers which possess foraminifer, nannofossil, and detrital calcite contents of about 5%, 50%, and 20%, respectively (Fig. 8). A trace fossil assemblage that is rich in *Zoophycus* is found throughout this subunit. Only one 5-cm-thick turbidite layer was encountered in Subunit IIIA (Core 117-730A-24X, 227.7 mbsf). It is composed mainly of tests of planktonic foraminifers and contains some pyrite grains at its base.

A number of subvertical joints several centimeters long that display small-scale offsets were found throughout this sequence. The most spectacular feature is a steeply dipping fault zone in Sample 117-730A-24X-4, 70 cm (225.4 mbsf). It displays several smeared faults, one of which may show reverse faulting (Figs. 9 and 10).

Subunit IIIB (Depth: 239.6–347.1 m)

Subunit IIIB is a pelagic foraminifer-bearing nannofossil chalk and marly chalk that is interrupted by slump horizons and calcareous turbidites; the latter are composed of foraminifer silts and sands. Four larger slump horizons, each roughly 1.5–2 m thick, are recognized in Cores 117-730A-26X (239.5–242.2 mbsf), -28X (262.4–263.8 mbsf), -31X (294–296.2 mbsf), and -37X (345.9–347.1 mbsf). The turbidites are interbedded with the pelagic chalks and the slump horizons and have an abundance of one to four turbidites per core. Turbidites are more common and have a larger grain size in the lower part of this section (Cores 117-730A-32X to -36X, 297.6–347.1 mbsf).

The colors of the chalks range from white (5Y 8/1) to light gray (5Y 7/2) to olive gray (5Y 5/2). Carbonate contents vary between 50% and 95% (Fig. 5), and organic carbon contents are below 1%. Foraminifers occur with an abundance of roughly 10% (Fig. 8).

The composition of the slump horizons is similar to the underlying and overlying chalks. The slumps are 1.5–2 m thick and often display laminated shear zones 20–50 cm thick at the base. This is followed by a zone composed of overturned folds separated by minor shear surfaces (Figs. 11, 12, and 13).

The frequency of the foraminifer-bearing turbidites as well as their content of large shallow-water foraminifers increases downsection. Turbidites in Cores 117-730A-25X to -28X (223–

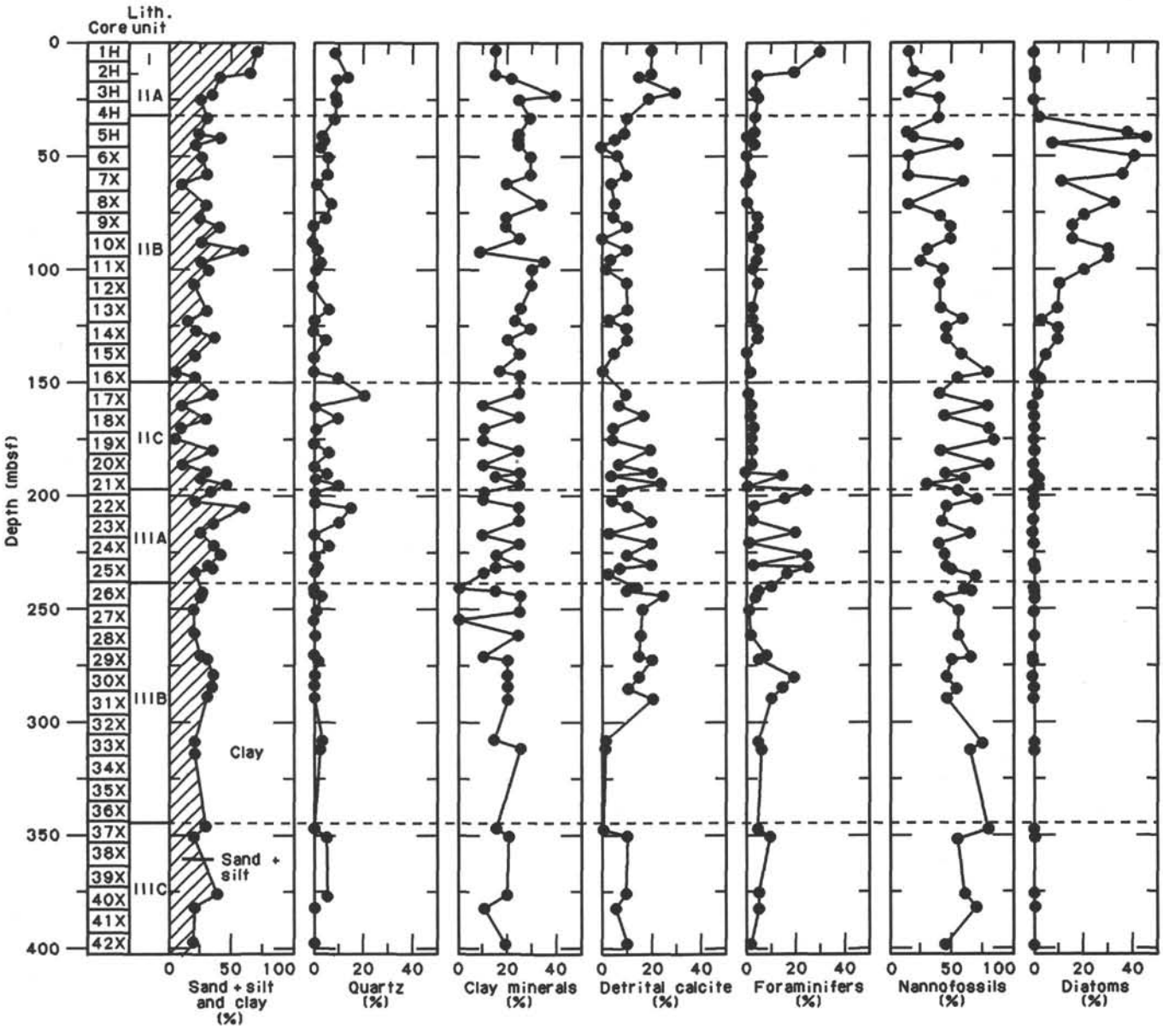

Figure 8. Smear slide data for Site 730, in area percent.

269 mbsf) are composed mainly of planktonic and minor amounts of benthic foraminifers and range from a few centimeters thick up to 20 cm thick. However, turbidites from Core 117-730A-29X to -36X (269–346 mbsf) are thicker and display a higher amount of large nummulitic foraminifers with a diameter of 0.5 cm. Those layers have a sharp base and show grading and imbrication.

In Core 117-730A-36X the nummulitic turbidites contain a small percentage of black, rounded clay intraclasts (0.5 cm diameter) with a few percentage of nannofossils that are the same age as the pelagic intervals. Thin sections show an isopachous rim cement in the chambers of planktonic foraminifers in Cores 117-730A-22X through -35X (259–326 mbsf). However, *Nummulitidae* of the turbidites, which are originally composed of high-magnesium calcite (Bathurst, 1975), display a much higher degree of dissolution and syntaxial calcite overgrowth.

Subunit IIIC (Depth: 347.1–403.9 m)

Subunit IIIC is composed of foraminifer-bearing marly nannofossil chalk to chalk and contains only a few turbidites in comparison to Subunit IIIB. The chalk exhibits a light-dark layering that ranges in color from white (5Y 8/1) to light gray (5Y 7/1) to olive gray (5Y 4/2). Some of the dark layers are thin and have a nodular appearance due to the presence of compacted, partly cemented burrows (Figs. 14 and 15). In the carbonate-rich layers, cross sections of less-compacted burrows show diffuse haloes, possibly of pyrite, which give the rock a spotty appearance (Fig. 14).

Only a few turbidites were encountered (Cores 117-730A-40X and -42X). They are between 10 and 35 cm thick and are composed entirely of benthic foraminifer sands.

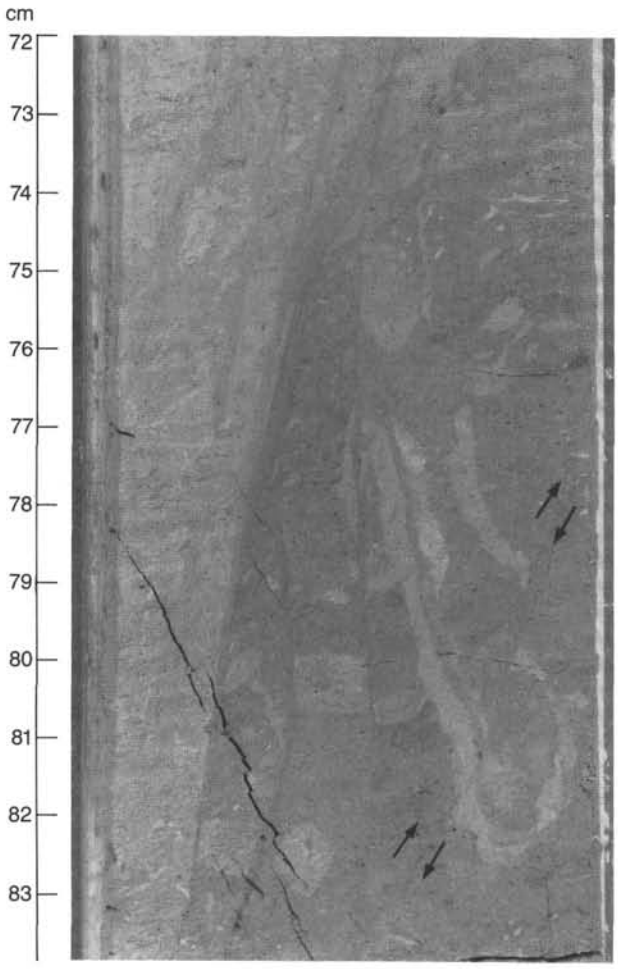

Figure 9. Steeply dipping faults with smeared fault planes. Offset of burrow in lower right corner seems to indicate reverse faulting in Subunit IIIA (Section 117-730A-24X-4, 72–84 cm).

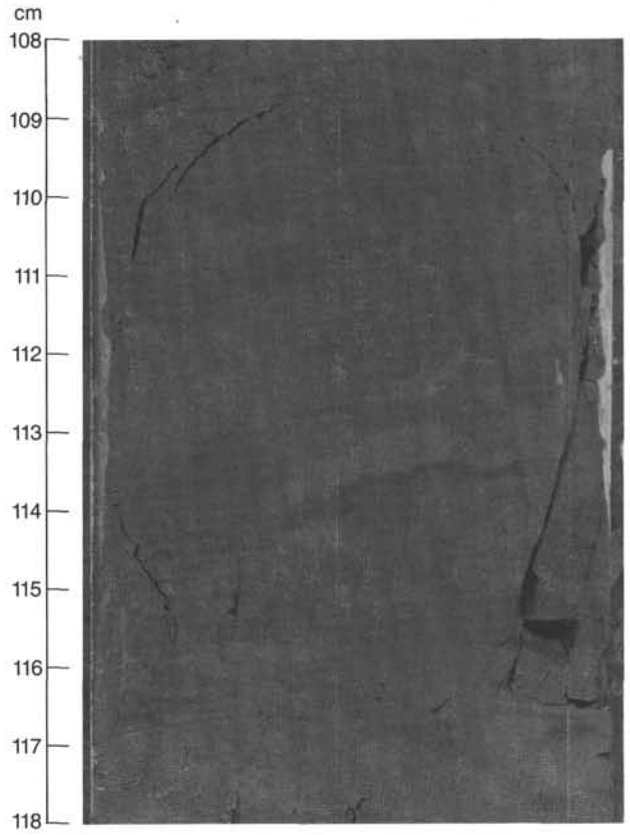

Figure 10. Set of subvertical joints that show a small offset in the bioturbation pattern of Subunit IIIA (Section 117-730A-24X-6, 108–118 cm).

Discussion

The following observations are worth mentioning regarding the environment and tectonic development of Site 730.

1. The turbidites found in Unit III indicate decreasing turbidite activity upsection. They document a trend from relatively proximal, thick, sandy turbidites with large shallow-water foraminifers toward thin, distal turbidites that contain dominantly planktonic and benthic foraminifers. This may indicate the gradual drowning of an isolated source area with abundant large-foraminifer sands and shallow-water environments. Other explanations may include the gradual uplifting of Site 730 to a more isolated position in the basin or other changes in paleogeography.
2. Slump horizons document tectonic activity during the lower part of the middle Miocene, which may indicate a syndepositional phase of steepening seafloor at Site 730. However, faulting may have continued from the middle Miocene into the Holocene.
3. The hiatus encountered between Unit I and Unit II indicates a considerable period of nondeposition and supposed erosion that ended in the Pleistocene. The hiatus may document the generation of relief combined with tectonic uplift.
4. The carbonate curve at Site 730 displays a generally decreasing trend through the early to late Miocene. The curve shows the change from relatively high values (85%) at the end of the early Miocene to relatively low values (30%–50%) at the beginning of the late Miocene. This trend was also noticed for the Owen Ridge sites (Sites 721, 722, and 731). It documents the transition from an environment that is dominated by the production of calcareous nannofossils to a system that is dominated by terrigenous input.

BIOSTRATIGRAPHY

Introduction

Site 730 is located in water depths of 1065 m on the Oman margin to the east of a ridge that separates two of the sedimentary basins on the upper slope. Abundant calcareous nannofossils and benthic foraminifers with good preservation are found in the uppermost three samples (0–27.3 mbsf). Below this level down to 258.9 mbsf, benthic foraminifers are few to rare, but with good to moderate preservation. Nannofossils are abundant, usually with moderate preservation. Below 258.9 mbsf benthic foraminifers are few to rare, but the preservation has been affected by calcitic recrystallization and lithification. Nannofossils in this interval are heavily overgrown, especially the asteroliths. Planktonic foraminifers are abundant with good preservation in the uppermost sample (8.3 mbsf). In Cores 117-730A-2H through -16X (17.8–152.6 mbsf), planktonic foraminifers are few and poorly preserved. Below 152.6 mbsf their abundance increases and preservation improves to moderate and good.

Siliceous microfossils are absent in the uppermost three core-catcher samples (0–27.3 mbsf). From 36.8 to 191.2 mbsf radiolarians are common and well preserved. From 200.9 to 278.2

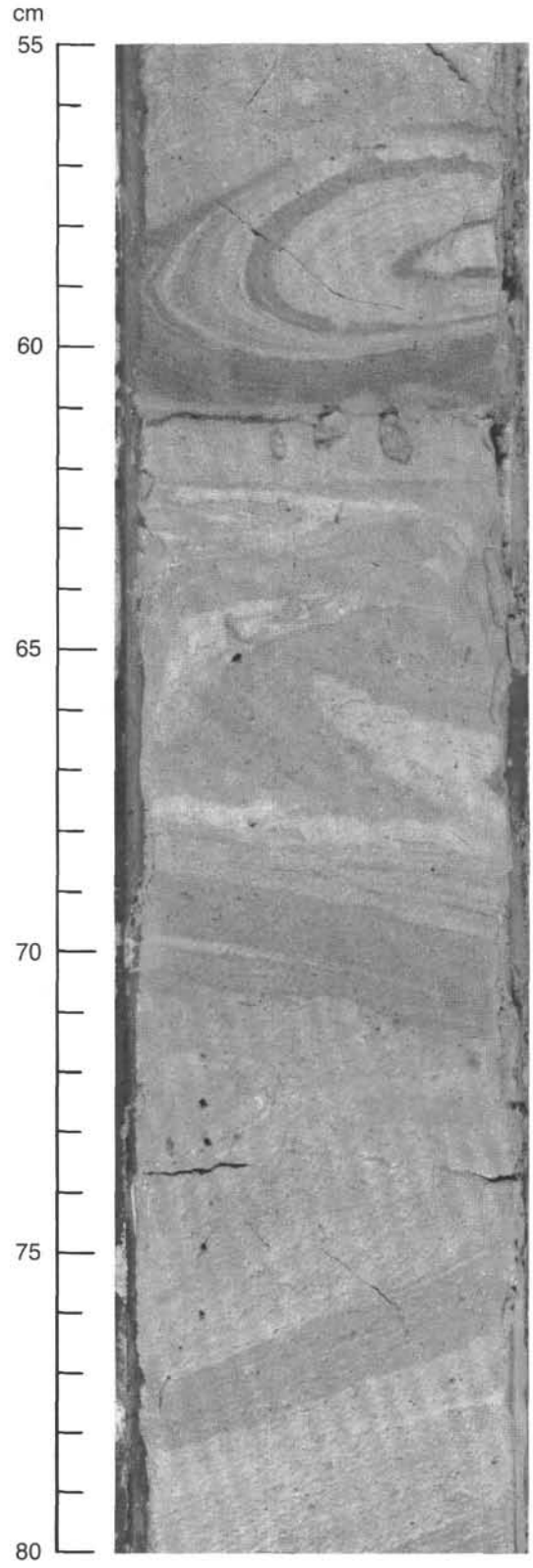

Figure 11. Upper portion of a slump horizon displaying overturned folds in Subunit IIIB (Section 117-730A-26X-1, 55–80 cm).

mbsf their abundance decreases and preservation is moderate. Diatoms and sponge spicules are present in the interval of radiolarian occurrences; below 278.2 mbsf no siliceous microfossils were found. A synopsis of microfossil zonations is presented in Figure 16.

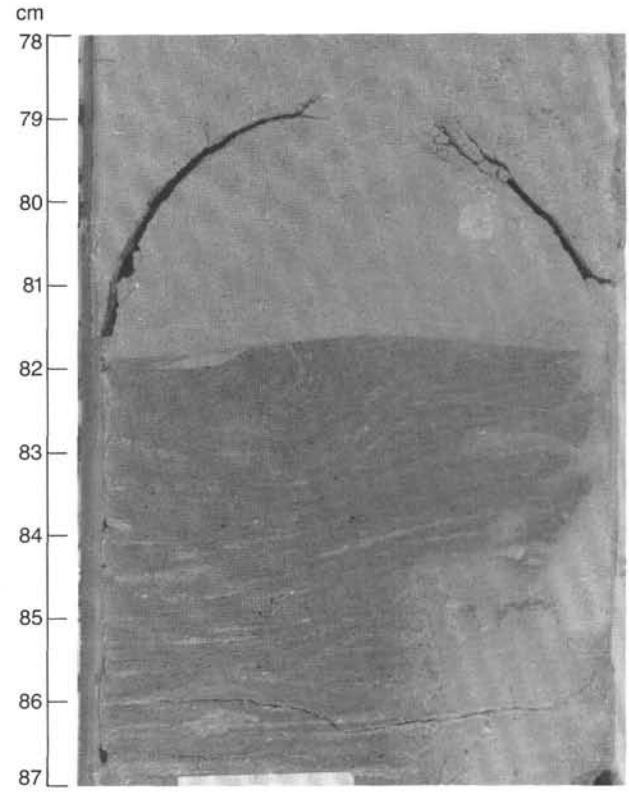

Figure 12. Shear horizons in the lower portion of the slump depicted in Figure 11. The horizon shows an offset in the bioturbation pattern of Subunit IIIB (Section 117-730A-26X-2, 78–87 cm).

A pronounced hiatus was recognized between 15.35 and 17.8 mbsf. Most of the Pleistocene, all of the Pliocene, and part of the upper Miocene are missing. A plot of faunal datum levels vs. depth below sea floor is presented in Figure 17; for a detailed listing of these data points see Table 3.

Planktonic Foraminifers

We studied planktonic foraminifers in core-catcher samples from Hole 730A. The first sample (117-730A-1H, CC; 8.3 mbsf) contains a highly diverse Pleistocene fauna (N23), and the preservation of tests is good.

A few moderately well-preserved specimens were found in Samples 117-730A-2H, CC, through 117-730A-16X, CC (17.8–152.6 mbsf). This part of the recovered sequence is assigned to the upper and middle Miocene and points to a hiatus somewhere in Core 117-730A-2H. Sample 117-730A-2H, CC, yields rare occurrences of *Globorotalia tumida plesiotumida* or *Globorotalia tumida merotumida*, which are zonal markers for N16–N17 (upper Miocene). Samples 117-730A-3X, CC, through 117-730A-9X, CC (27.3–86.4), are barren. Zones N13–N14 (middle Miocene), exemplified by the presence of *Globorotalia siakensis*, were recognized in Samples 117-730A-13X, CC, through 117-730A-16X, CC (123.5–154.0 mbsf). No attempts were made to discern the zonal boundary between N13 and N14, which is defined by the first appearance of *Globigerinoides nepenthes*, because this species was only found in highly scattered occurrences.

Below Sample 117-730A-16X, CC (152.6 mbsf), planktonic foraminifers are common to abundant and moderately well preserved. The *Globorotalia fohsi* evolutionary lineage (Zones N10–N12) was found in Samples 117-730A-17X, CC, through 117-730A-31X, CC (162.2–297.6 mbsf). The zonal boundaries are tentative because they are based on first appearances of the

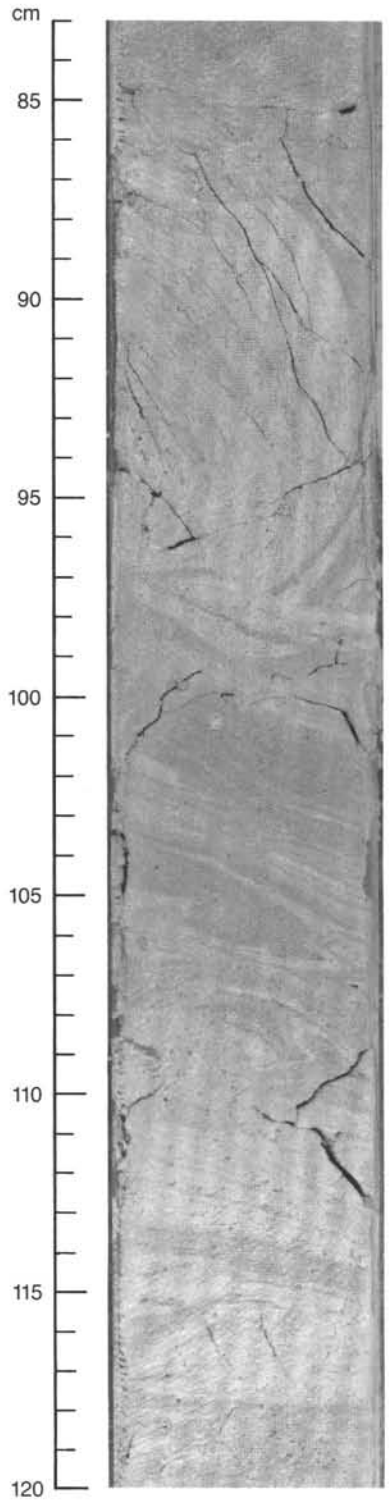

Figure 13. Upper portion of slump horizon displaying shear surfaces and overturned folds in Subunit IIIB (Section 117-730A-31X-5, 83–120 cm).

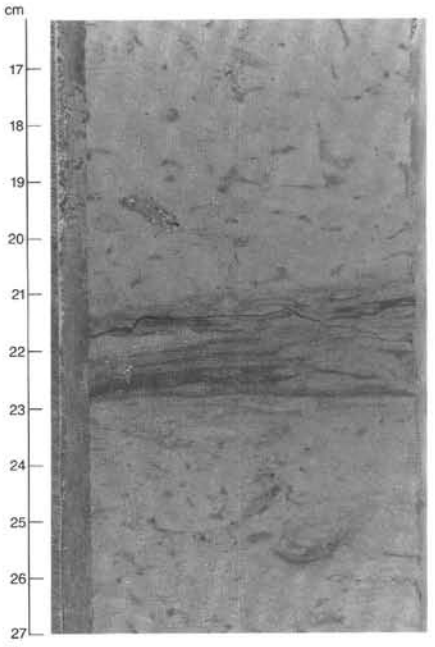

Figure 14. Diagenetic alternations of bedding chalk. Haloed, little compacted burrows in the chalk layers are contrasted by compacted nodular burrows in the clay-rich layers of Subunit IIIC (Section 117-730A-40X-1, 16–27 cm).

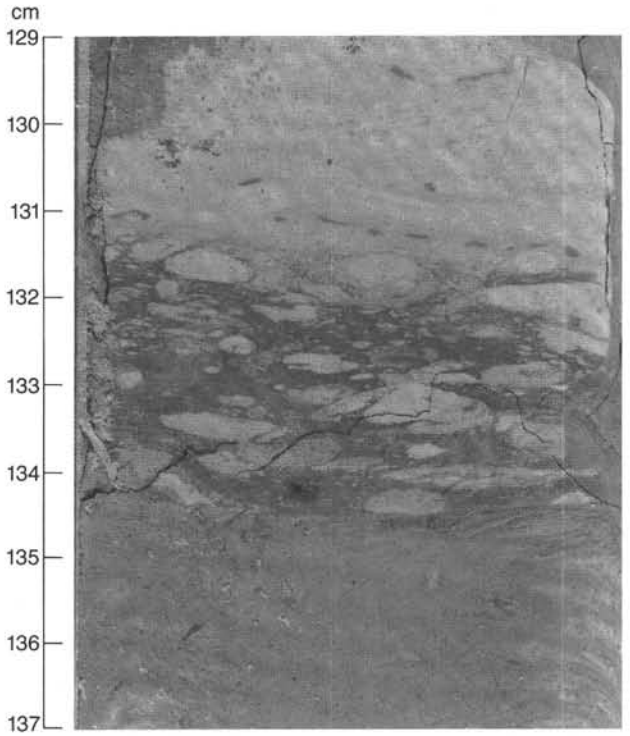

Figure 15. Nodular character of a relatively clay-rich layer that exhibits flattened burrow cross sections with high carbonate content in Subunit IIIC (Section 117-730A-40X-6, 129–137 cm).

morphologic transitional series from *Globorotalia peripheronda* to fully developed *Globorotalia fohsi*. The first appearance of *Orbulina universa*, which marks the lower limit of Zone N9, was found in Sample 117-730A-31X, CC (297.6 mbsf).

The basal part of the recovered section, Samples 117-730A-32X, CC, through 117-730A-42X, CC (307.2–403.9 mbsf), is referred to lower Miocene Zone N8. *Globigerinoides sicanus* is present and *Orbulina universa* is absent in these sediments.

Benthic Foraminifers

The abundance of benthic foraminifers in core-catcher samples from Hole 730A is high only in the upper three samples

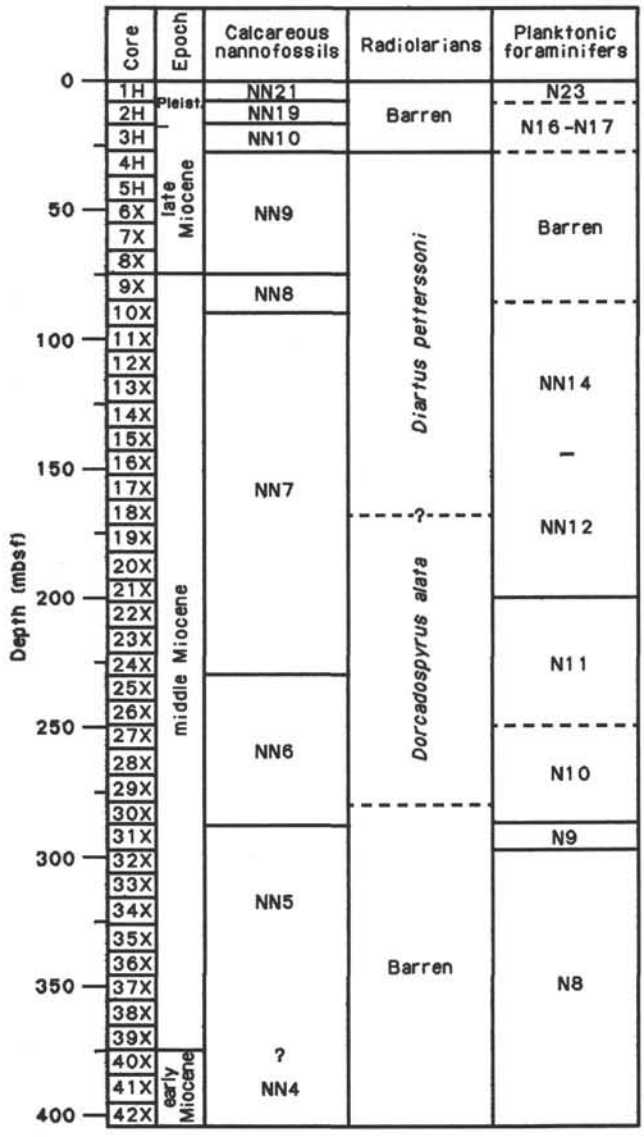

Figure 16. Correlation of planktonic microfossil zones in Hole 730A.

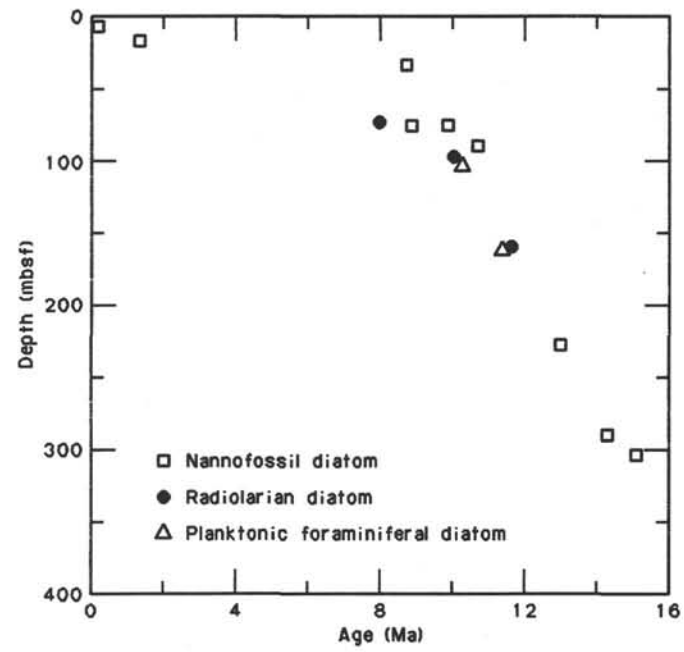

Figure 17. Age-depth plot for Hole 730A. For a detailed listing of the events, see Table 3.

(117-730A-1H, CC, through -3H, CC; 8.3–27.3 mbsf), which corresponds approximately to the interval of marly nannofossil ooze (Unit I). Below Sample 117-730A-3H, CC (27.3 mbsf), abundance ranges from few to rare, and preservation is good to moderate for most of the sequence. Calcitic recrystallization in combination with lithification of the sediments below Sample 117-730A-27X, CC (258.9 mbsf), affects preservation in the part of the sequence studied.

The planktonic/benthic (P/B) ratio is variable. It decreases gradually from more than 99 in the uppermost sample (117-730A-1H, CC; 8.3 mbsf) to 0 in Sample 117-730A-6X, CC (55.8 mbsf); it remains low down to Sample 117-730A-19X, CC (181.6 mbsf). An exception for an excursion exists up to about 90 around 100 mbsf. Below Sample 117-730A-19X, CC (181.6 mbsf), the P/B ratio is consistently higher than 90.

The benthic foraminiferal fauna of Site 730 is quite uniform. An upper middle bathyal faunal assemblage is found throughout the sequence. It is characterized by the presence of *Bulimina truncana, Cibicidoides wuellerstorfi, Hoeglundina elegans, Melonis barleeanum,* and *Pullenia bulloides* in most samples. Species which are present in lower relative abundance are *Bulimina mexicana, Sigmoilinopsis schlumbergeri, Sphaeroidina bulloides,* and *Uvigerina auberiana.*

Below Sample 117-730A-24X, CC (229.9 mbsf), thick turbidite sequences occur which contain such shallow-water species as *Amphistegina* spp. and *Elphidium macellum*; nummulitids are common as well.

Calcareous Nannofossils

Nannofossils are abundant throughout Hole 730A. Sediments down to Sample 117-730A-1H, CC (8.3 mbsf), contain abundant specimens of *Emiliania huxleyi* and are assigned to Zone NN21 (uppermost Pleistocene to Holocene). The presence of *Pseudoemiliania lacunosa* and *Gephyrocapsa caribbeanica* in Sample 117-730A-2H-5, 105–106 cm, assigns these sediments to the Pleistocene part of Zone NN19. The presence of *Sphenolithus abies, Reticulofenestra pseudoumbilica,* and such discoasters as *D. brouweri, D. pentaradiatus, D. neohamatus,* and *D. pansus* places Sample 117-730A-2H, CC, in Zone NN10 (upper Miocene). Therefore, the lower part of Zone NN19 and Zones NN18 through NN11 are missing somewhere between 15.35 mbsf and 17.8 mbsf.

Samples down to 117-730A-4H-3, 105–106 cm (31.35 mbsf), contain the same species as in 117-730A-2H, CC, together with *Discoaster calcaris* and *D. bollii* and may also be assigned to Zone NN10. Nannofossils exhibit good preservation in the three uppermost samples. The top of *Discoaster hamatus* occurs between Samples 117-730A-4H-3, 105–106 cm, and 117-730A-4H-5, 105–106 cm, and marks the top of Zone NN9. The total range of *D. hamatus* defines Zone NN9. The bottom of this fossil occurs between Samples 117-730A-8X, CC, and 117-730A-9X-1, 105–106 cm (75.20–76.25 mbsf). In this zone, sporadic occurrences of *Catinaster calyculus* and *C. coalitus* are recognized.

Sediments below 76.25 mbsf down to the bottom of *Catinaster coalitus* are assigned to middle Miocene Zone NN8. Samples 117-730A-10X-5, 105–106 cm, down to 117-730A-24X-5, 105–106 cm (91.95–227.25 mbsf), belong to Zone NN7 (middle Miocene) based on the absence of *C. coalitus* and the presence of *Discoaster kugleri.* The age of the boundary between Zones NN8

Table 3. Stratigraphic listing of faunal events for Hole 730A.

	Event	Core, section, interval (cm)	Depth (mbsf)	Age (Ma)	Source of age
B	*Emiliania huxleyi*	117-730A-1H, CC	8.30	0.19	3
		117-730A-2H-1, 117-118	8.82		
B	*Geophyrocapsa* "large"[a]	117-730A-2H-5, 105-106	15.35	[b]1.36	4
		117-730A-2H, CC	17.80		
T	*Discoaster hamatus*	117-730A-4H-3, 105-106	31.35	8.85	6
		117-730A-4H-5, 105-106	34.35		
T	*Stichocorys wolffii*	117-730A-8X-4, 85-87	70.85	[c]8.0-8.2	2
		117-730A-8X, CC	75.20		
T	*Catinaster coalitus*	117-730A-8X, CC	75.20	9.0	6
		117-730A-9X-1, 105-106	76.25		
B	*Discoaster hamatus*	117-730A-8X, CC	75.20	10.0	6
		117-730A-9X-1, 105-106	76.25		
B	*Catinaster coalitus*[d]	117-730A-10X-3, 105-106	88.95	10.8	6
		117-730A-10X-5, 105-106	91.95		
T	*Cyrtocapsella japonica*	117-730A-10X, CC	94.60	10.0-10.3	2
		117-730A-11X-4, 85-87	99.95		
T	*Globorotalia mayeri*	117-730A-11X-4, 65-67	99.75	10.4	6
		117-730A-11X, CC	104.25		
T	*Lithopera thornburgi*	117-730A-16X, CC	152.60		
		117-730A-17X-4, 85-87	157.65		
T	*Cyrtocapsella cornuta*	117-730A-17X-4, 85-87	157.95	11.6-11.9	2
		117-730A-17X, CC	162.20		
T	*Globorotalia fohsi*	117-730A-17X, CC	162.20	11.5	6
		117-730A-18X-2, 65-67	164.35		
B	*Diartus petterssoni*	117-730A-18X-4, 85-87	167.55		
		117-730A-18X, CC	171.90		
T	*Lithopera renzae*	117-730A-19X-4, 85-87	177.25		
		117-730A-19X, CC	181.60		
B	*Discoaster kugleri*	117-730A-24X-5, 105-106	227.25	13.1	6
		117-730A-24X, CC	229.90		
T	*Sphenolithus heteromorphus*	117-730A-30X, CC	287.90	14.4	6
		117-730A-31X-1, 105-106	288.95		
B	*Orbulina universa*	117-730A-31X-3, 65-67	291.55	15.2	6
		117-730A-31X, CC	297.60		

Note: T = upper limit of event and B = lower limit. Sources of ages are: 2 = Johnson and Nigrini, 1985; 3 = oxygen isotope data for Site 723 (N. Niitsuma, unpubl. data); 4 = Takayama and Sato, 1987; and 6 = Berggren et al., 1985.

[a] Long axis greater than 6 μm.
[b] North Atlantic data.
[c] Pacific Ocean data.
[d] Should be lower.

and NN7 was estimated by Berggren et al. (1985) as 10.8 Ma. In Hole 730A, this datum coincides with the highest occurrence of *Coccolithus miopelagicus.* Samples 117-730A-24X, CC, through 117-730A-30X, CC (229.9–287.9 mbsf), belong to Zone NN6 (middle Miocene) based on the absence of *Discoaster kugleri* and *Sphenolithus heteromorphus.*

Bukry's (1973) zonation shows the last appearance datum (LAD) of *Cyclicargolithus floridanus* coinciding with the first appearance datum (FAD) of *Discoaster kugleri* (NN7/NN6 boundary). According to Bukry (1975), however, the LAD of *C. floridanus,* which is often used as a surrogate criterion for the NN7/NN6 boundary, is within Zone NN7 as defined by the FAD of *D. kugleri* in some areas, including Site 563 (North Atlantic). In the present hole, however, the LAD of *C. floridanus* is clearly recognizable and coincides with the FAD of *D. kugleri.* Nannofossil preservation ranges from good to poor, with moderate preservation between 36.8 and 249.2 mbsf in most samples.

Below 249.2 mbsf the preservation of the coccoliths becomes abruptly poorer and almost all specimens, especially asteroliths, are heavily overgrown. Below 287.9 mbsf, sediments down to the bottom of the hole (Samples 117-730A-31X, CC, through -42X, CC) contain *Sphenolithus heteromorphus,* together with *C. floridanus* and *Discoaster deflandrei. Discoaster druggii* and sporadic occurrences of *Hayaster perplexus* are also recognized. Because *Helicosphaera ampliaperta* is not recognized in this hole, these sediments are assigned to Zones NN5 and NN4 (middle to lower Miocene).

Radiolarians

Radiolarians are common and well preserved in the samples from Cores 117-730A-4H through -20X (36.8–191.2 mbsf). They decrease in abundance, and preservation is only moderate between Samples 117-730A-21X, CC, and 117-730A-25X-4, 85–87 cm (200.9–235.25 mbsf). From Sample 117-730A-25X, CC, to Sample 117-730A-29X, CC (239.6–278.2 mbsf), there is a further decrease in abundance and even more deterioration in the preservation state. Both above and below these intervals, the recovered sediments are barren of siliceous microfossils. Diatoms and sponge spicules are common to abundant thoughout the silica-rich interval. Sponge spicules are particularly robust, but they do show pitting due to dissolution in the sections where radiolarians are less abundant.

From Samples 117-730A-4H-4, 85–87 cm, to 117-730A-18X-4, 85-87 cm (32.65–167.55 mbsf), the radiolarians belong to the *Diartus petterssoni* Zone. The FAD of *D. petterssoni* is in Sample 117-730A-18X-4, 85-87 cm, and this event normally marks the *D. petterssoni/Dorcadospyris alata* zonal boundary. Thus, the sediments from Samples 117-730A-18X, CC, to 117-730A-29X, CC (171.9–278.2 mbsf), appear to belong to the *D. alata* Zone. However, the LAD of *Liriospyris parkeri* and *D. alata* should also coincide approximately with this boundary, but we observed neither of these species. In addition, placement of the *D. petterssoni/D. alata* boundary between Samples 117-730A-18X-4, 85–87 cm, and 117-730A-18X, CC (168.35–171.9 mbsf), is inconsistent with the nannofossil zonal data.

Paleoenvironmental Implications

The occurrence of rare *Globigerina bulloides* specimens and the first appearance of biogenic silica during the middle Miocene indicates that upwelling conditions were present in this area at that time. These conditions may be related to the onset of the monsoon system. However, a full analysis of the planktonic foraminiferal and radiolarian faunas found at Oman margin Site 730 is necessary to establish the onset and variations in the monsoon system during the Miocene.

PALEOMAGNETISM

Magnetic Measurements

We measured the archive halves of Cores 117-730A-1H through -5H on the pass-through cryogenic magnetometer after alternating-field (AF) demagnetization at 5 mT. The records were again dominated by high scatter and incompletely removed coring overprints, and no useful information was obtained. Figure 18 shows the results of MINISPIN measurements of discrete samples (after AF demagnetization at 5 or 10 mT) for the interval from 0 to 150 mbsf. Only samples with circular standard deviations (CSDs) of $<40°$ are plotted.

A major hiatus occurs within Core 117-730A-2H (8.3–17.8 mbsf) separating sediments of Pleistocene and late Miocene age. Intensities average around 0.5 mA/m over the interval from 40 to 110 mbsf and are slightly lower both above and below. The most striking aspect of the records is the long normally magnetized interval between about 50 and 110 mbsf, spanning nannofossil Zones NN9 through NN7; the upper part may be correlative with Chron C5 (Chronozone 11).

Magnetic Susceptibility

The volume magnetic susceptibility of Hole 730A sediments was measured on the Bartington Susceptibility Meter (Model MS1) and a whole-core, pass-through sensor coil at the 0.1 sen-

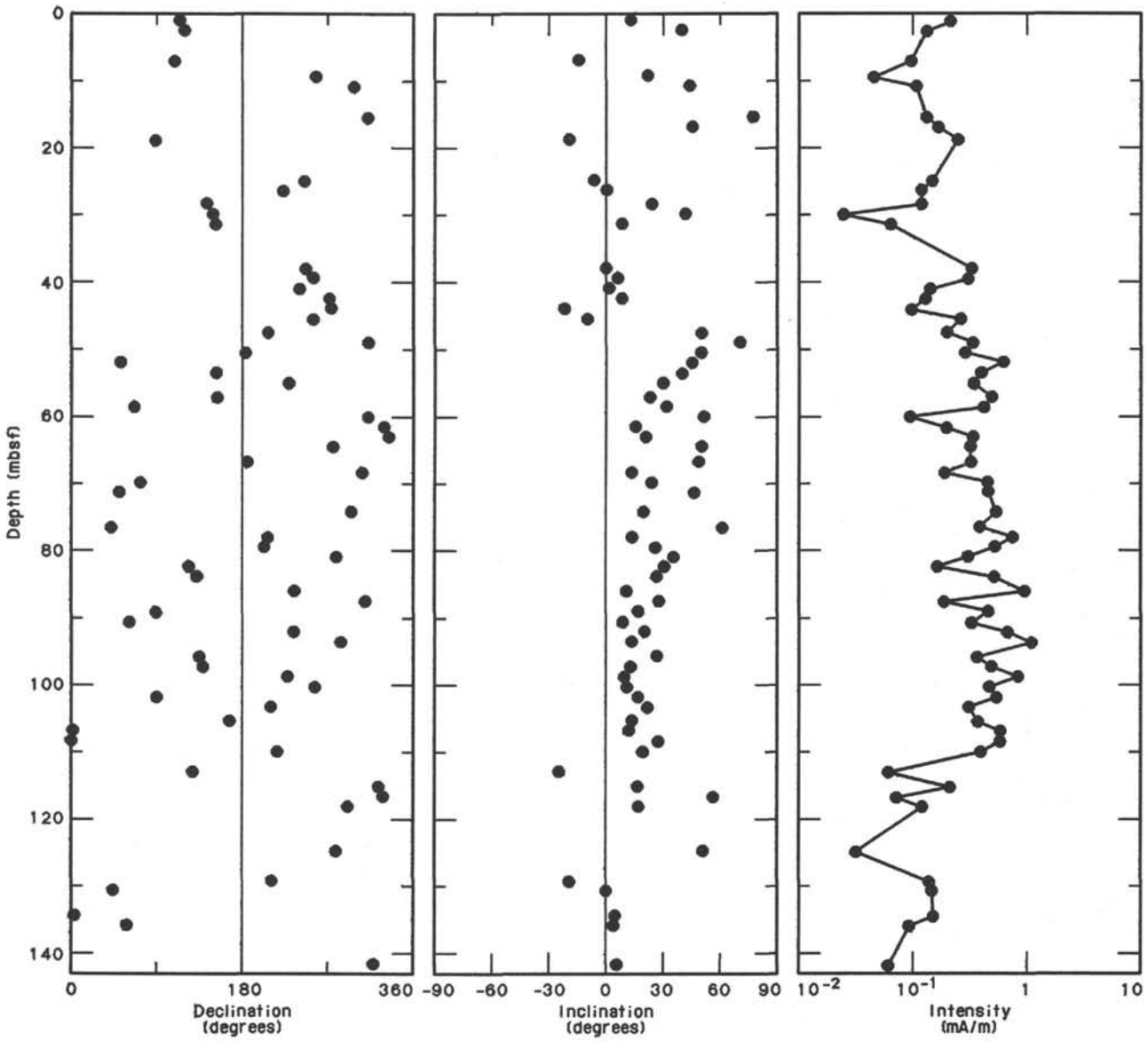

Figure 18. Declination, inclination, and intensity for discrete samples from Hole 730A, after 5–10 mT demagnetization. Only samples with circular standard deviations (CSDs) of $<40°$ are plotted.

sitivity and 0.47 kHz low-frequency settings. Hole 730A was cored with the APC to Core 117-730A-5H (46.3 mbsf) and cored in the XCB mode from Cores 117-730A-6X to -42X (403.9 mbsf). Measurements were performed at 8-cm intervals. Susceptibility data vary from ~25 to 140 × 10^{-6} SI units (Fig. 19).

Sedimentological investigations have indicated three lithologic units (see "Lithostratigraphy" section, this chapter). Unit I consists of a marly nannofossil ooze that extends from the top to 15.2 mbsf. A disconformable hiatus spanning nannofossil Zones NN21–NN10 was found in Core 117-730A-2H at the base of Unit I (see "Biostratigraphy" section, this chapter). Although the hiatus is not conspicuous sedimentologically, the susceptibility data are very high (~200 × 10^{-6} SI units) over the interval containing the hiatus horizon. The susceptibility peak is centered at Sample 117-730A-2H-5, 70 cm, or 15.00 mbsf.

Although core-top pipe rust contamination is apparent in most XCB cores, this interval of high susceptibility is within Core 117-730A-2H; therefore, the data most probably reflect real changes in the concentration and grain size of ferrimagnetic grains. A tentative conclusion, which is consistent with the visual descriptions of Core 117-730A-2H, is that this horizon is a coarse lag-type deposit from a previous erosional or failure event.

Unit II extends from 15.2 to 201.0 mbsf and comprises marly nannofossil oozes and diatomaceous silty clays of late to middle Miocene age. Most of the sediments in Unit II were recovered by XCB coring, and rust contamination is common, as evidenced by the regular ~10-m spikes. Structure within the susceptibility data of Unit II is apparent, but sedimentological interpretations are wanting in the absence of detailed data. Preliminary comparisons of the susceptibility data and the visual core descriptions did not indicate any simple associations.

Unit III extends from 201.0 to 403.9 mbsf and is dominated by foraminifer-bearing nannofossil chalks. The susceptibility data of Unit III are somewhat lower in value than those of Unit II. However, as with Unit II, we could establish no simple relationships between susceptibility data and core descriptions.

ACCUMULATION RATES

Sedimentation rates for Site 730 are based on the biostratigraphic datum levels listed in Table 3. We recognized a pronounced hiatus between 15 and 18 mbsf, which represents almost 8 m.y. of missing section (see "Biostratigraphy" section, this chapter). Because of poor stratigraphic control above the hiatus, only the FAD of *Emiliania huxleyi* was used to estimate the mean rate of sedimentation in the late Pleistocene (44 m/m.y.; Fig. 20). Based on a best fit to the biostratigraphic datums, the mean sedimentation rate was 49 m/m.y. in the interval from 8 to 15 Ma (Fig. 20). Therefore, the late Pleistocene and Miocene rates of sediment accumulation at Site 730 are similar. These values are also similar to rates determined in pelagic sediments of comparable age on the Owen Ridge (see Owen Ridge site chapters, this volume).

PHYSICAL PROPERTIES

Introduction

Physical properties measured on discrete samples of sediments recovered from Site 730 include index properties (wet-bulk density, porosity, water content, and grain density), compressional-wave velocity, and vane shear strength. The properties that were determined for discrete samples are listed in Table 4. Wet-bulk density and compressional-wave velocity were measured on all whole-round core sections longer than 80 cm using the GRAPE and *P*-wave logging systems. All techniques and equipment used are described in the "Explanatory Notes" (this volume).

The relatively high recovery rate at Site 730 provided a high sampling frequency. With this large data set, we could distinguish the boundaries between the three lithologic units identified at Site 730 by the transitions in the physical properties profiles.

Index Properties

Unit I

Relatively little change in index properties is displayed in the thin interval of marly nannofossil foraminifer ooze that makes up Unit I (0–15.2 mbsf; Fig. 21). Average values for porosity, water content, wet-bulk density, and grain density in Unit I are 63%, 39%, 1.67 g/cm^3, and 2.66 g/cm^3, respectively.

Unit II

Unit II (15.2–201.0 mbsf) is characterized by the occurrence of high porosity and water content and low grain and wet-bulk density in association with an increased abundance of siliceous microfossils and organic matter. Transitions in the index property profiles mark the boundaries between nannofossil silty clay to marly nannofossil ooze (Subunit IIA), diatomaceous marly nannofossil ooze (Subunit IIB), and marly nannofossil ooze (Subunit IIC).

Index-property profiles for Subunit IIA (15.2–33.2 mbsf) show increases in porosity from 57% to 72% and in water content from 33% to 49%; wet-bulk density, on the other hand, decreases from 1.76 to 1.50 g/cm^3 with increasing depth (Fig. 21). These changes reflect the downsection decrease in grain size in this interval. Grain density is 2.60 g/cm^3 at the top and bottom of Subunit IIA; however, it decreases from the top of Subunit IIA to a minimum value of 2.48 g/cm^3 at 26.1 mbsf (Fig. 21). The low grain density at this depth coincides with a minimum in the calcium carbonate percentage (Fig. 5).

Subunit IIB (33.2–150.45 mbsf) contains sediment with the highest porosity and water content and lowest wet-bulk density and grain density at Site 730. Between 33.2 and 62.6 mbsf, porosity and water content are essentially constant, with average values of 78% and 58%, respectively. Grain density varies from 2.45 and 2.22 g/cm^3 in this interval and is accompanied by variations in wet-bulk density from 1.41 to 1.33 g/cm^3 (Fig. 21). The interval from 33.2 to 62.6 mbsf contains the highest abundance of diatoms and radiolarians at Site 730 (see "Biostratigraphy" section, this chapter) and organic carbon percentages as high as 3.39% (see "Organic Geochemistry" section, this chapter).

Because of their low grain densities and high water retentiveness, the abundant siliceous microfossils and organic material are responsible for the high porosity and water content and low densities. From 62.6 mbsf to the base of Subunit IIB, there is a progressive decrease in diatom and radiolarian abundance which is accompanied by decreases in porosity (from 78% to 71%) and water content (from 60% to 47%) as well as by increases in grain density (from 2.22 to 2.66 g/cm^3) and wet-bulk density (from 1.33 to 1.55 g/cm^3). The pattern of increasing grain and wet-bulk density is reversed between 92.9 and 109.5 mbsf (Fig. 21). Minimum values of grain density (2.36 g/cm^3) and wet-bulk density (1.40 g/cm^3) in this interval correspond to a peak in organic carbon concentration (4.04%) at 106.5 mbsf.

The downsection trends of decreasing porosity and water content and increasing grain and wet-bulk density that characterize the lower portion of Subunit IIB are reversed in Subunit IIC (120.1–150.5 mbsf). The top of Subunit IIC is marked by slight decreases in porosity and water content; wet-bulk density increases from 1.55 to 1.66 g/cm^3. Grain density changes only slightly across the boundary between Subunit IIB and IIC, decreasing from 2.66 to 2.64 g/cm^3. Normal compaction trends resume between 137.9 mbsf and the base of Subunit IIC, and porosity decreases to 66%, water content decreases to 41%, and

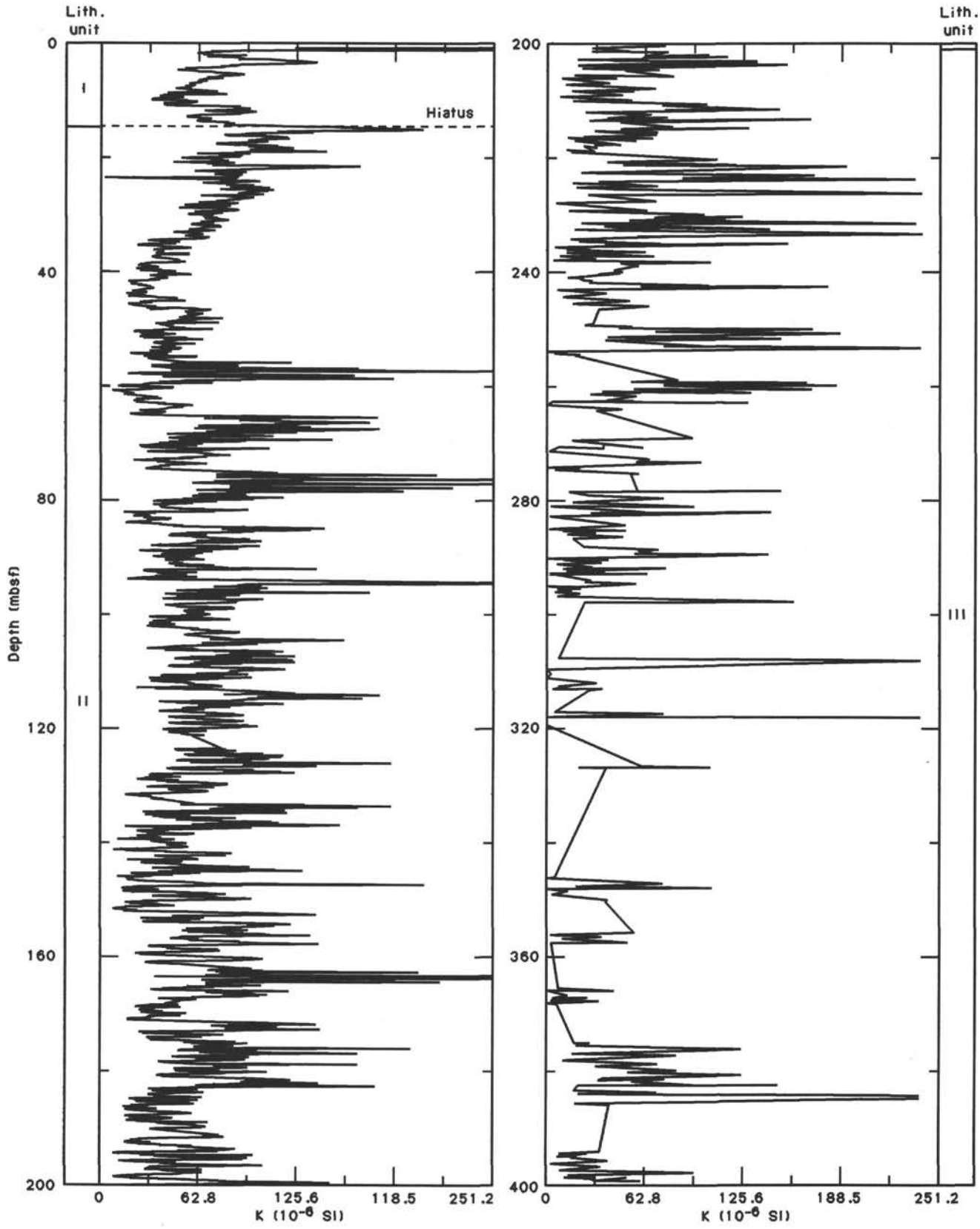

Figure 19. Magnetic susceptibility (K) data for Hole 730A.

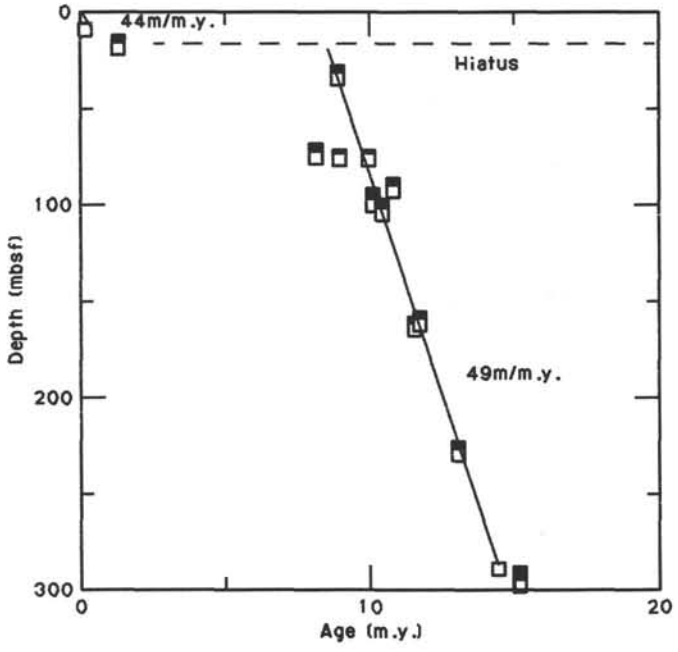

Figure 20. Age-depth plot of stratigraphic datums listed in Table 3. The filled and open boxes are the upper and lower depths of each datum level, respectively. The sedimentation rates indicated are calculated from a best fit of the reliable datums.

grain and wet-bulk density increase to 2.71 and 1.64 g/cm^3, respectively (Fig. 21).

Unit III

The marly nannofossil ooze/chalk and foraminiferal nannofossil chalk of Unit III (201.0–403.9 mbsf) are characterized by a uniform decrease in porosity and water content and increase in wet-bulk density with increasing depth. Boundaries between the five subunits of Unit III cannot be distinguished on the basis of index properties. Index-property profiles for Unit III are divided into two segments by gradient changes that occur at approximately 294 mbsf (Fig. 21). In the interval between 201.0 and 293.6 mbsf, there is a gradual decrease in porosity from 62% to 53% and in water content from 38% to 29%. There is a concomitant rise in wet-bulk density from 1.67 to 1.86 g/cm^3.

Concentrations of siliceous microfossils and organic carbon decrease over this interval, but because of their low initial value there is only a slight increase in grain density from 2.59 to 2.64 g/cm^3. From 293.6 mbsf to the bottom of Hole 730A (403.9 mbsf), gradients are reduced as porosity and water content decrease to 44% and 23%, respectively, and wet-bulk density increases to 1.96 g/cm^3. Grain density is essentially constant below 293.6 mbsf with an average value of 2.65 g/cm^3. Siliceous microfossils are absent below 289.7 mbsf; and, as a consequence of the lack of significant compositional variation, changes in porosity, water content, and wet-bulk density primarily reflect sediment compaction in response to increasing overburden pressure.

Two well-lithified chalks were sampled in Unit III at 272.3 mbsf (Sample 117-730A-29X-3, 65–67 cm) and 285.5 mbsf (Sample 117-730A-30X-6, 58–60 cm). These rocks are characterized by anomalously low porosity and water content and low wet-bulk density (Fig. 21 and Table 4).

Compressional-Wave Velocity

Compressional-wave velocity was measured on discrete samples from all three lithologic units at Site 730, including not only the indurated chalks but also the lower density nannofossil oozes and diatomaceous silty clays (Table 4 and Fig. 21). Within Units I and II compressional-wave velocity shows relatively little variation and a consistent trend of increasing velocity with depth from approximately 1500 m/s near the seafloor to 1575 m/s at the base of Unit II. This increase in compressional-wave velocity reflects a relatively rapid increase in wet-bulk density with depth from <1.4 to 1.6 g/cm^3 (Figs. 21 and 23).

Within the nannofossil oozes and chalks of Unit III, the variation in compressional-wave velocity increases significantly. This variation is most likely the result of differences in relative abundances of clay minerals, foraminifers, and nannofossils as well as sharp changes in the degree of induration encountered in this sequence of interbedded ooze and chalk. The affect of induration on compressional-wave velocity is illustrated by two samples of exceptionally well-indurated chalk (Samples 117-730A-29X-3, 65–67 cm, and 117-730A-30X-5, 125–127 cm), where the velocities measured perpendicular to bedding are 2078 and 2450 m/s, respectively. These values deviate significantly from the general velocity-depth profile (Fig. 22).

The relationship between velocity and density for the sequences at Site 730 shows a well-defined trend that closely matches the empirical correlation of Hamilton (1978) for calcareous sediments and chalks (Fig. 23). Variation of the data on the velocity-density crossplot is similar to that shown on the velocity-depth profile. The diatomaceous silty clays and diatomaceous marly nannofossil oozes of Unit II, all with densities of 1.6 g/cm^3 or less, show a well-defined velocity–density relationship. In contrast, the relationship between the marly nannofossil oozes/chalks and the foraminiferal nannofossil chalks of Unit III is characterized by a markedly higher variation, with no consistent relationship between velocity and calcium carbonate content.

Anisotropy of the compressional-wave velocity for 36 samples of chalk from Unit III shows no consistent relationship to either density or sub-bottom depth. Eight percent of the samples displayed small negative anisotropies (velocity parallel to bedding less than that perpendicular to bedding) that probably resulted from errors in measurement if the surfaces of the samples were not exactly parallel. Anisotropy of the remaining 33 samples ranged from 0.1% to 5.5%, with a mean of 1.7%.

GRAPE and *P*-Wave Logs

Continuous GRAPE wet-bulk density data were determined to a depth of approximately 290 mbsf at Site 730. Reliable data were obtained for Cores 117-730A-1H to -16X (0–152 mbsf). From the seafloor to 152 mbsf, the GRAPE wet-bulk densities correlate well with the wet-bulk density measurements obtained from discrete samples (Fig. 24). The transition from Unit I to Unit II (15.2 mbsf) is clearly shown as a drop in the wet-bulk density from 1.70 to 1.65 g/cm^3. The boundary from Subunit IIA to Subunit IIB (33.2 mbsf) is shown by a decrease from 1.50 to 1.40 g/cm^3. The transition from Unit II to Unit III (201.0 mbsf) is evidenced by an increase in the density/depth gradient, as also noted in the discrete samples.

The quality of the GRAPE data diminishes from Core 117-730A-17X to Core 117-730A-42X as the result of a decrease in the recovered core diameter giving smaller density values. Therefore, at depths greater than 152 mbsf the discrete sample data are consistently higher than the GRAPE wet-bulk density data by 0.5 to 1.5 g/cm^3. However, both sets of data continue to track along the same gradients.

The cyclic variations in the GRAPE data are not very well defined since the cycle intervals vary considerably with depth. The thickness of the intervals are on the order of 1–2 m. This trend corresponds to the smaller-scale cyclic variations evident at Sites 721 and 722.

Reliable compressional-wave velocity measurements with the *P*-wave logger were obtained from Cores 117-730A-1H to -10X

Table 4. Physical properties summary for Hole 730A.

Core, section, interval (cm)	Depth (mbsf)	Wet-bulk density (g/cm^3)	Porosity (%)	Water content (%)	Grain density (g/cm^3)	Dry-bulk density (g/cm^3)	Velocity (m/s)	Vane shear strength (kPa)
117-730A-								
1H-3, 78–80	3.78	1.643	64.9	40.5	2.656	0.978		
1H-5, 78–80	6.78	1.706	59.0	35.4	2.634	1.102		
2H-2, 78–80	10.58	1.612	66.1	42.0	2.697	0.935		
2H-4, 30–32	13.10							10.5
2H-4, 78–80	13.58	1.721	61.0	36.3	2.647	1.096		
2H-6, 78–80	16.58	1.761	56.7	33.0	2.601	1.179		
2H-7, 30–33	17.60						[a]1517	
3H-2, 130–132	20.60	1.639	65.5	40.9	2.709	0.968		
3H-4, 80–82	23.10	1.570	65.9	43.0	2.529	0.895		46.1
3H-6, 80–82	26.10	1.600	64.1	41.1	2.478	0.943	[a]1446	
4H-2, 78–80	29.58	1.597	64.8	41.6	2.537	0.932		
4H-4, 78–80	32.58	1.503	72.2	49.2	2.602	0.764		
4H-7, 8–10	36.38							106.9
4H-7, 17–19	36.47	1.382	79.6	59.0	2.653	0.567	[a]1467	
5H-2, 80–82	39.10	1.369	79.3	59.3	2.449	0.557		
5H-4, 80–82	42.10	1.342	78.3	59.8	2.282	0.540		
5H-6, 78–80	45.08	1.414	73.9	53.5	2.329	0.657	[a]1537	182.6
6X-2, 105–107	48.85	1.342	79.6	60.8	2.427	0.526		
6X-4, 80–82	51.60	1.370	76.1	56.9	2.367	0.591		
6X-6, 92–94	54.72	1.343	77.5	59.1	2.250	0.549	[a]1502	
7X-1, 130–132	57.10	1.338	80.3	61.5	2.409	0.515		
7X-3, 69–71	59.49	1.407	75.7	55.1	2.446	0.632	[a]1525	
7X-5, 80–82	62.60	1.333	77.7	59.7	2.217	0.537	[a]1533	
8X-2, 109–111	68.09	1.492	73.8	50.7	2.553	0.736	[a]1543	
8X-4, 103–105	71.03	1.511	68.6	46.5	2.468	0.808		
8X-6, 73–75	73.73	1.465	72.7	50.8	2.433	0.721		
9X-2, 78–80	77.48	1.490	72.7	50.0	2.552	0.745		
9X-4, 90–92	80.60	1.553	66.3	43.7	2.546	0.874	[a]1542	
9X-6, 140–142	84.10	1.487	70.6	48.7	2.463	0.763		
10X-2, 78–80	87.18	1.519	68.3	46.0	2.449	0.820		
10X-4, 78	80	90.18	1.447	75.2	53.3	2.519	0.676	
10X-6, 47–49	92.87	1.463	71.2	49.9	2.360	0.733	[a]1570	
11X-2, 110–112	97.20	1.397	74.2	54.4	2.368	0.637		
11X-4, 71–73	99.81	1.636	63.0	39.5	2.570	0.991		
11X-6, 69–71	102.79	1.597	66.2	42.5	2.618	0.919	[a]1540	
12X-2, 78–80	106.48	1.526	69.4	46.6	2.497	0.815		
12X-4, 78–80	109.48	1.618	62.9	39.8	2.505	0.974		
12X-6, 76–78	112.46	1.521	70.4	47.4	2.600	0.800		
13X-2, 127–129	116.67	1.548	70.7	46.8	2.662	0.824		
13X-5, 85–87	120.75	1.662	62.0	38.2	2.644	1.027	[a]1563	
14X-2, 78–80	125.78	1.686	59.7	36.3	2.593	1.074		
14X-4, 61–63	128.61	1.629	63.2	39.8	2.559	0.981		
14X-6, 64–67	131.64	1.593	64.7	41.6	2.534	0.930	[a]1577	
15X-2, 31–33	135.01	1.539	67.4	44.9	2.570	0.848		
15X-4, 23–25	137.93	1.501	73.8	50.4	2.622	0.745		
15X-6, 30–32	141.00	1.572	66.2	43.1	2.543	0.894		
16X-2, 14–16	144.54	1.640	65.3	40.8	2.695	0.970		
16X-4, 26–28	147.66	1.642	66.1	41.2	2.709	0.965		
16X-6, 24–26	150.64	1.476	69.8	48.5	2.378	0.760		
16X-6, 104–107	151.44						[a]1538	
17X-2, 73–75	154.83	1.668	62.2	38.2	2.587	1.030		
17X-4, 70–72	157.80	1.636	63.1	39.5	2.539	0.990		
17X-6, 58–61							[a]1650	
17X-6, 63–65	160.73	1.651	63.0	39.1	2.557	1.005		
18X-2, 36–38	164.06	1.665	62.9	38.7	2.656	1.021		
18X-4, 30–32	167.00	1.810	56.7	32.1	2.726	1.230		
18X-6, 32–34	170.02	1.635	62.7	39.3	2.520	0.993		
19X-2, 60–62	174.00	1.733	57.8	34.2	2.589	1.140		
19X-4, 80–82	177.20	1.728	61.3	36.3	2.714	1.100		
19X-6, 60–62	180.00	1.733	61.0	36.1	2.732	1.108		
19X-6, 62–64	180.02						[a]1632	
19X-6, 62–64	180.02						[b]1655	
20X-2, 93–95	184.03	1.681	61.5	37.5	2.658	1.051	[a]1586	
20X-2, 93–95	184.03						[b]1619	
20X-4, 96–98	187.06	1.690	61.7	37.4	2.655	1.058	[a]1557	
20X-4, 96–98	187.06						[b]1570	
20X-6, 50–52	189.60	1.717	59.0	35.2	2.630	1.113		
21X-2, 78–80	193.48	1.747	59.5	34.9	2.712	1.137		
21X-4, 44–46	196.14	1.645	62.2	38.7	2.598	1.008	[a]1562	
21X-4, 44–46	196.14						[b]1597	
21X-6, 69–71	199.39	1.747	55.5	32.6	2.618	1.178	[a]1661	
21X-6, 69–71	199.39						[b]1705	
22X-2, 123–125	203.63	1.747	56.7	33.2	2.591	1.167	[a]1655	

Table 4 (continued).

Core, section, interval (cm)	Depth (mbsf)	Wet-bulk density (g/cm^3)	Porosity (%)	Water content (%)	Grain density (g/cm^3)	Dry-bulk density (g/cm^3)	Velocity (m/s)	Vane shear strength (kPa)
117-730A- (Cont.)								
22X-2, 123-125	203.63						[b]1690	
22X-4, 120-122	206.60	1.717	60.5	36.1	2.691	1.097	[a]1614	
22X-4, 120-122	206.60						[b]1606	
22X-6, 57-59	208.97	1.800	56.8	32.3	2.730	1.218	[a]1699	
22X-6, 57-59	208.97						[a]1701	
23X-2, 88-90	212.98	1.783	57.4	33.0	2.789	1.195	[a]1696	
23X-2, 88-90	212.98						[b]1719	
23X-4, 94-96	216.04	1.754	56.2	32.8	2.629	1.178		
23X-6, 120-122	219.30	1.662	62.7	38.6	2.634	1.020	[a]1576	
23X-6, 120-122	219.30						[b]1608	
24X-2, 71-73	222.41	1.725	59.0	35.1	2.675	1.120	[a]1665	
24X-2, 71-73	222.41						[b]1703	
24X-4, 21-23	224.91	1.752	60.5	35.4	2.736	1.132	[a]1677	
24X-4, 21-23	224.91						[b]1688	
24X-6, 47-49	228.17	1.773	56.2	32.5	2.653	1.198	[a]1724	
24X-6, 47-49	228.17						[b]1762	
25X-2, 87-89	232.27	1.705	58.9	35.4	2.630	1.101	[a]1651	
25X-2, 87-89	232.27						[b]1664	
25X-4, 107-109	235.47	1.768	59.0	34.2	2.736	1.164	[a]1632	
25X-4, 107-109	235.47						[b]1659	
25X-6, 84-86	238.24	1.832	54.4	30.5	2.708	1.274	[a]1739	
25X-6, 84-86	238.24						[b]1794	
26X-2, 102-104	242.12	1.819	56.0	31.5	2.783	1.245	[a]1632	
26X-2, 102-104	242.12						[b]1643	
26X-4, 72-74	244.82	1.862	52.6	29.0	2.706	1.322	[a]1787	
26X-4, 72-74	244.82						[b]1799	
27X-2, 27-29	250.97	1.768	56.5	32.7	2.758	1.189	[a]1616	
27X-2, 27-29	250.97						[b]1620	
27X-4, 91-93	254.61	1.820	57.4	32.3	2.724	1.232		
28X-1, 137-139	260.27	1.799	56.2	32.0	2.724	1.223	[a]1609	
28X-1, 137-139	260.27						[b]1643	
28X-4, 80-82	264.20	1.813	55.2	31.2	2.677	1.247	[a]1655	
28X-4, 80-82	264.20						[b]1665	
29X-2, 31-33	270.41	1.844	55.1	30.6	2.785	1.280	[a]1668	
29X-2, 31-33	270.41						[b]1714	
29X-3, 65-67	272.25	2.001	45.0	23.0	2.741	1.541	[a]2078	
29X-3, 65-67	272.25						[b]2197	
29X-5, 70-72	275.30	1.778	56.0	32.3	2.600	1.204	[a]1657	
29X-5, 70-72	275.30						[b]1683	
30X-5, 125-127	285.45	2.070	38.5	19.0	2.634	1.676	[a]2450	
30X-5, 125-127	285.45						[b]2434	
30X-6, 58-60	286.28	1.763	57.9	33.6	2.652	1.171	[a]1609	
30X-6, 58-60	286.28						[b]1633	
31X-1, 87-89	288.77	1.716	60.0	35.8	2.696	1.101		
31X-4, 124-126	293.64	1.855	52.8	29.1	2.639	1.315	[a]1684	
31X-4, 124-126	293.64						[b]1661	
31X-6, 53-55	295.93	1.855	53.8	29.7	2.699	1.304	[a]1699	
31X-6, 53-55	295.93						[b]1700	
32X-1, 48-50	298.08	1.932	48.4	25.7	2.658	1.436		
33X-1, 29-31	307.49	1.833	53.4	29.8	2.618	1.287	[a]1674	
33X-1, 29-31	307.49						[b]1702	
33X-5, 2-4	313.22	1.888	50.0	27.1	2.688	1.376	[a]1691	
33X-5, 2-4	313.22						[b]1709	
34X-1, 50-52	317.40	1.834	54.0	30.2	2.640	1.280	[a]1697	
35X-1, 17-19	326.37	1.922	50.2	26.7	2.585	1.408		
37X-1, 81-83	346.71	1.846	52.1	28.9	2.641	1.313	[a]1683	
37X-1, 81-83	346.71						[b]1706	
37X, CC, 30-32	350.45	1.903	52.1	28.0	2.626	1.370		
38X-2, 21-23	357.31	1.875	52.7	28.8	2.704	1.335		
39X-1, 75-77	365.95	1.860	53.2	29.3	2.679	1.315	[a]1631	
39X-1, 75-77	365.95						[b]1646	
39X-2, 92-94	367.62	1.883	52.1	28.4	2.684	1.349	[a]1683	
39X-2, 92-94	367.62						[b]1731	
40X-2, 20-22	376.60	1.845	52.9	29.4	2.639	1.303		
40X-4, 53-55	379.93	1.940	49.9	26.3	2.781	1.429	[a]1803	
40X-4, 53-55	379.93						[b]1871	
41X-1, 54-56	385.14	1.688	47.3	28.7	2.698	1.204	[a]1653	
41X-1, 54-56	385.14						[b]1641	
42X-1, 98-100	395.18	1.875	46.3	25.3	2.574	1.400	[a]1887	
42X-1, 98-100	395.18						[b]1918	
42X-3, 16-18	397.36	1.963	44.1	23.0	2.543	1.512	[a]2031	
42X-3, 16-18	397.36						[b]2057	

[a] Velocity measurement perpendicular to bedding.
[b] Velocity measurement parallel to bedding.

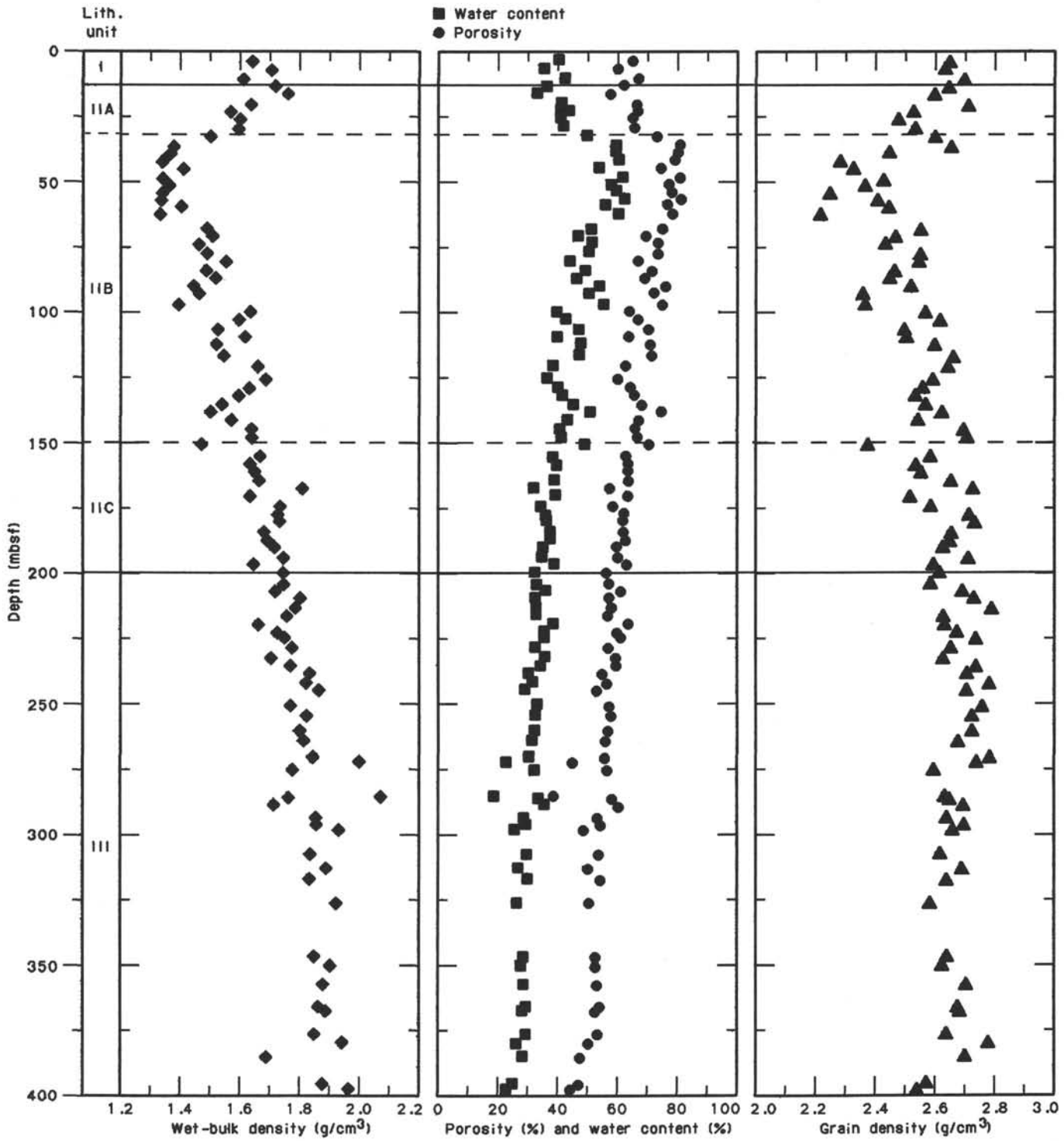

Figure 21. Index properties (wet-bulk density, porosity, water content, and grain density) measured on discrete samples for Hole 730A.

(0–95 mbsf; Fig. 25). We were unable to determine *P*-wave data for the interval from 95 to 135 mbsf since the sediments were not making sufficient contact with the core liner. The *P*-wave logger data display a trend similar to that contained in the GRAPE records. However, the density minimum zone seen in the GRAPE data between 25 and 75 mbsf is not reflected in the *P*-wave data.

The interval from 0 to 25 mbsf shows a decrease in compressional-wave velocity from 1575 m/s to 1550 m/s; from 25 to 95 mbsf the velocities average 1535 m/s. An increase in velocity from 1525 to 1675 m/s was measured in the interval from 135 to 250 mbsf. The *P*-wave logger data values are consistently less than the compressional-wave velocity measurements determined from discrete samples. The discrepancy between the discrete and

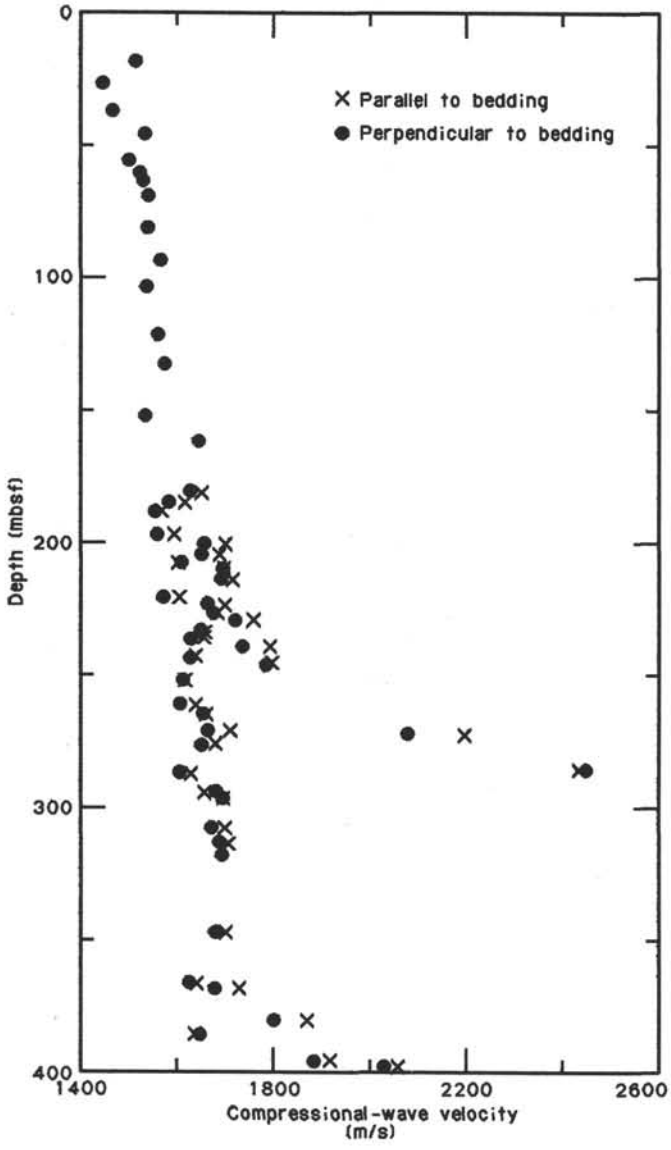

Figure 22. Compressional-wave velocity as measured on discrete samples in the Hamilton Frame Velocimeter for Hole 730A.

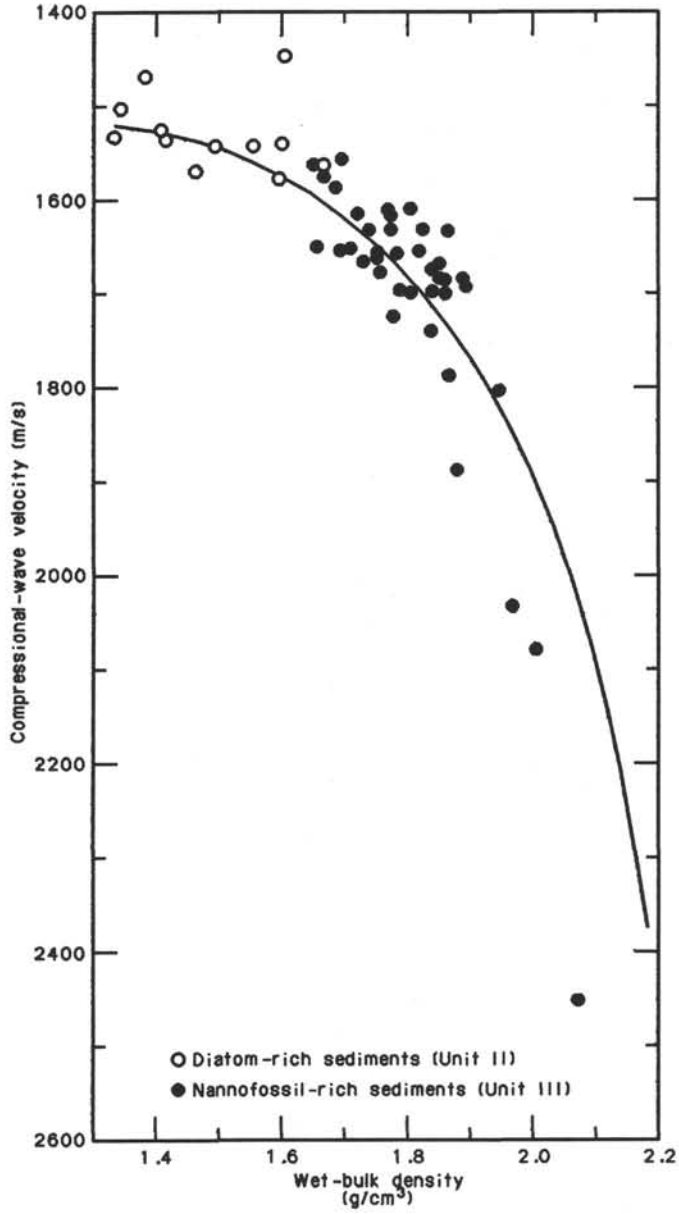

Figure 23. Wet-bulk density vs. compressional-wave velocity measured perpendicular to bedding on discrete samples. The solid line is an empirical correlation for velocity vs. density in calcareous marine sediments (30% calcium carbonate) from Hamilton (1978).

P-wave velocities results from the decrease in core diameter and an increase in drilling-induced sediment slurry surrounding intact sediment blocks.

Vane Shear Strength

Four vane shear strength measurements made on cores from the upper 45 m of the section at Site 730 (Table 4) define a consistent trend of rapidly increasing shear strength as well as a markedly higher rate of increase in shear strength below the hiatus in Cores 117-730-H-5. In the Pleistocene section (0–15.2 mbsf), vane shear strength increases at a rate of 0.80 kPa/m, as compared with an average rate of 6.3 kPa/m in the section underlying the Pleistocene/upper Miocene hiatus.

The consistently high shear strengths obtained from this section of Site 730 cores could be the result of previous burial to depths greater than present sub-bottom positions. However, because of the limited number of measurements at this site and the lack of comparable data from other sites on the Oman margin, any detailed interpretation of these results would be highly speculative.

SEISMIC STRATIGRAPHY

Site 730 is located on the slope of a submarine terrace which separates two slope basins that form the southeast corner of the Oman margin. Seismic features display patterns that might be critical for interpreting the evolution of the Oman margin.

The area between the two slope basins is displayed on the shipboard seismic line (Fig. 26) as an anticlinal structure with east- and westward-dipping reflectors. The western basin has a different pattern of reflectors than the slope-adjacent terrace, indicating different lithologies or ages for the western slope ba-

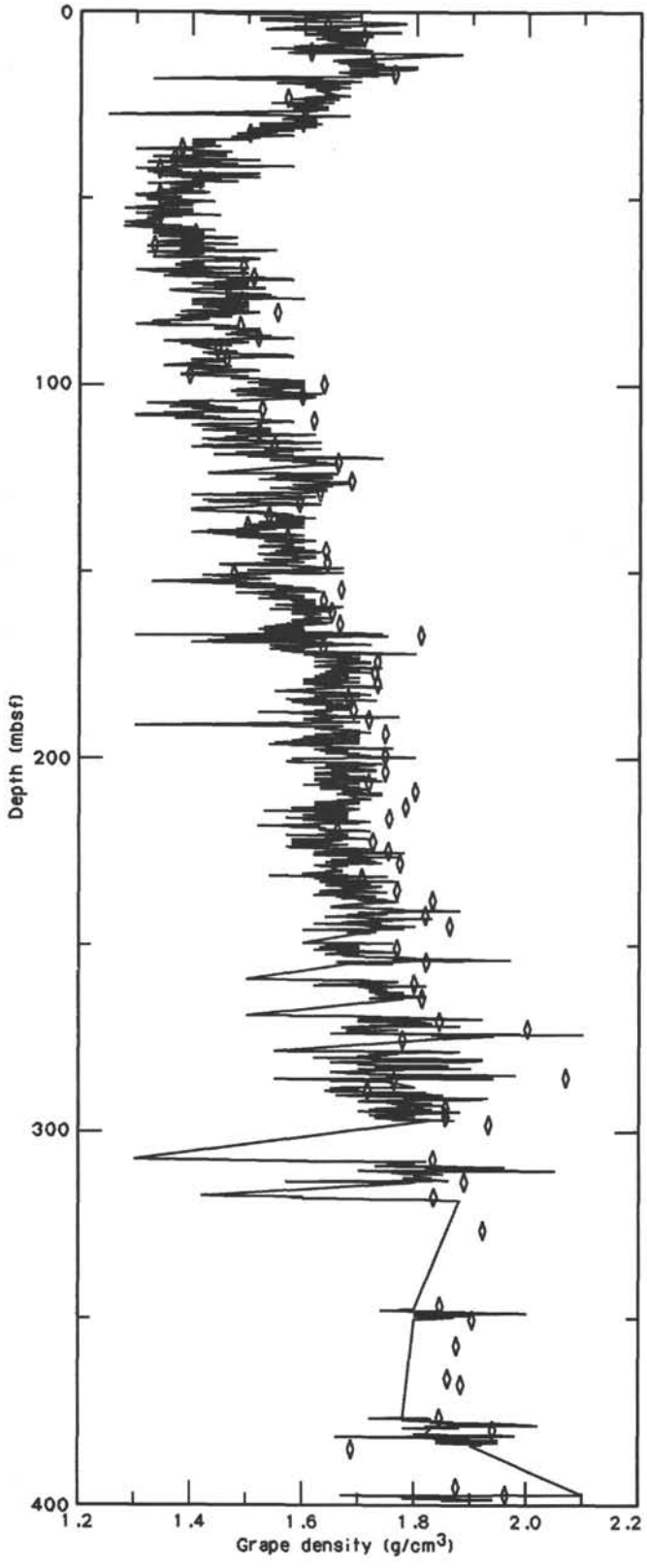

Figure 24. GRAPE wet-bulk density for Hole 730A. The profile is based on 10-cm-block averages of the data. Diamond-shaped symbols represent wet-bulk densities determined for discrete samples.

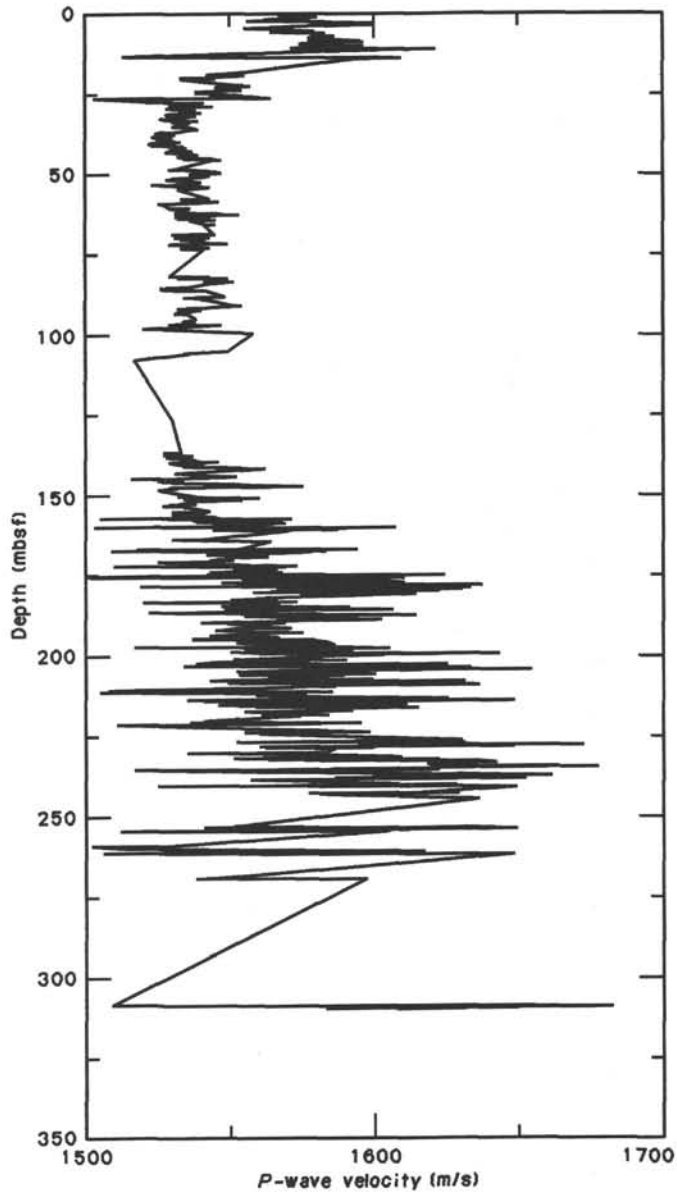

Figure 25. Compressional-wave velocity as measured by the *P*-wave logger for Hole 730A. The profile is based on 10-cm-block averages of the data.

sin and the slope terrace (Figs. 26 and 27). The detailed seismic connection between the two areas is unclear.

Seismic Unit A (Fig. 27) is a Quaternary sequence that forms a thin veneer over underlying sequences. This unit has parallel reflectors that are locally concordant as well as discordant to the underlying sequences. The thickness of this unit remains constant along the seismic section shown (Fig. 26).

Seismic Units B, C, and D (Fig. 27) belong to the Miocene section recovered at Site 730. Unit B has well-developed clinoforms with eastward-prograding reflectors. Older reflectors of Unit B are truncated by younger reflectors that produce onlap toward the east and toplap toward the center of the anticline.

Seismic Unit C has a uniform thickness and is a relatively homogeneous layer seismically, which seems to correlate with the upper portion of the chalk encountered at Site 730 (see "Lithostratigraphy" section, this chapter). At the top of the anticline,

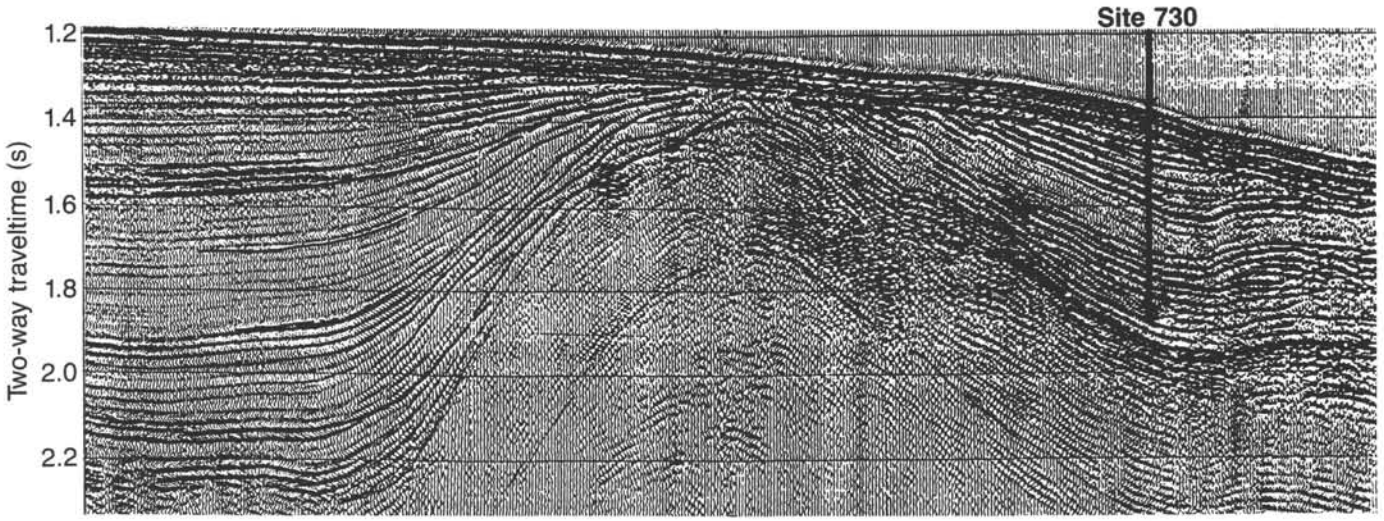

Figure 26. Seismic line on the submarine terrace showing location of Site 730. See Figure 2 for location of *JOIDES Resolution* Line 8.

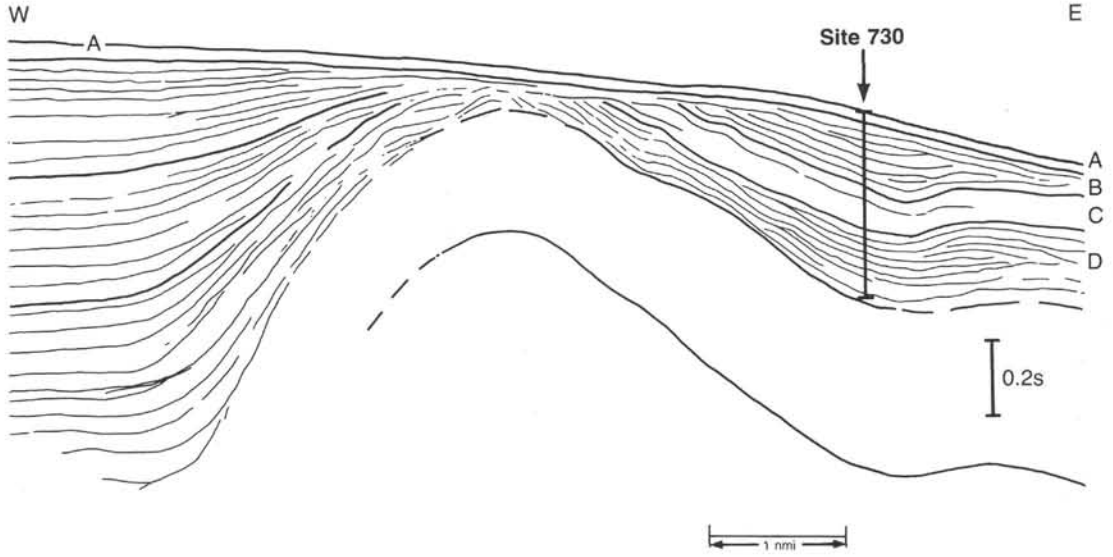

Figure 27. Schematic interpretation of Figure 26 showing seismic reflectors A–D.

some reflectors of seismic Unit C truncate older reflectors of this sequence and are in turn truncated by seismic Unit A.

Seismic Unit D, an eastward-thickening sequence, corresponds to middle and early Miocene chalks recovered at Site 730. Reflectors are discontinuous throughout this section and show numerous downlap and toplap patterns. At the top of the anticline, the reflectors appear to be irregular, wavy-shaped, and locally moundlike.

Discussion

The following observations seem to be critical for the interpretation of the basin development of the Oman margin.

Seismic Unit D is equivalent to middle to early Miocene chalks recovered at Site 730 which contains turbidites and slump horizons. This observation is consistent with the irregular patterns of truncating reflectors found in this unit. The lower portion of the turbidite-chalk sequence recovered at Site 730 contains redeposited, large benthic foraminifers, which could be derived from shallow-water carbonates developed at the top of the anticline, where wavy reflectors may indicate progradational lobes of carbonate sands. Unit D thickens eastward, suggesting that the depositional slope faced in this direction. If this conclusion is correct, seismic Unit D was a shallow-water facies (50–100 m water depth) only in the area of the top of the anticline.

Seismic Units B and C exhibit large-scale clinoforms, indicating progradation of sediment wedges to the east and leading to a contemporaneous overlapping of thin layers at the top of the anticline. It is not clear whether this overlap is related to erosional truncation followed by short phases of sedimentation or whether overlapping layers represent condensed equivalents of the thick Miocene sediments encountered at Site 730. The offlap pattern and overlap of thin layers on the anticline show that the shallow-water carbonates in seismic Unit D became somewhat submerged to allow a smooth veneer of sediment to occur on the anticline. This interpretation is supported by the waning occurrence of turbidite beds upsection in Site 730. On the other hand, submergence was not strong enough to develop a general draping pattern. Instead, the offlap pattern observed

may indicate outer shelf conditions with roughly 200–400 m of water depth.

While the western slope basin has well-developed sediments of Pliocene and Quaternary age, we did not find any equivalent sediments on the anticline near Site 730 except for the thin veneer of Quaternary sediments in Unit A. This phenomenon might be interpreted as being the result of a recent uplift with accompanying erosion or nondeposition.

INORGANIC GEOCHEMISTRY

Introduction

We collected 15 interstitial water samples by squeezing from Hole 730A. Analytical results are listed in Table 5 and are presented in Figures 28 and 29.

Salinity, Chloride, and pH

Salinity decreases with depth at this site (Fig. 28) as a direct consequence of the reduction of sulfate and loss of magnesium from solution between ~25 and ~200 mbsf. In contrast, no significant variation is seen in the chloride content (Fig. 28), and the pH varies only slightly between maximum and minimum values of ~7.7 and ~7.1 (Fig. 28). The pH is lower than that of seawater, probably as a consequence of the production of H_2S during sulfate reduction.

Alkalinity and Sulfate

The highest alkalinity measured at this location (~6.8 mmol/L at 110 mbsf) is significantly lower than is observed at most other Oman margin sites (Fig. 28). The greatest rate of addition of alkalinity to pore solution (i.e., greatest positive slope) coincides well with the maximum negative slope in the sulfate profile (Fig. 28). However, the absolute alkalinity concentration is much lower than should be present considering that sulfate is fully reduced at depth. This presumably reflects a high degree of removal of dissolved inorganic carbon from pore waters by precipitation of authigenic carbonates. The observed magnesium distribution supports this interpretation (see below). A second reason for the low alkalinity at depth is the relatively low ammonia content.

The depth at which the sulfate concentration goes to zero (~250 mbsf) is substantially greater at this site than that observed at nearby Site 727 (~55 mbsf). This contrast is most probably a function of the difference in sedimentation rate between the two locations. Sedimentation at Site 727 has apparently been continuous throughout the Pleistocene, whereas much of the Pleistocene and Pliocene are missing at Site 730. The high organic carbon concentrations present in the upper Miocene chalks clearly provide a metabolizable substrate for sulfate-reducing bacteria in Hole 730A, suggesting that, despite its age, the organic matter is still viable as an energy source for bacteria: it must have been preserved to some extent when it was initially buried during the late Miocene. However, the presence of dissolved sulfate at considerable depths in the hole, coupled with the associated relatively low ammonia concentrations, suggests that such preservation has been moderate at best. The shallower depth at which sulfate is fully depleted in Hole 727A is consistent with the implication that a higher oxidant demand is associated with the more rapidly buried (thus somewhat "fresher") organic matter at this site.

It is interesting to note that we found no indication in either the sulfate or chloride data for the presence of a relatively fresh, sulfate-enriched fluid at depth at this site, as there was at nearby Site 727. This contrast may arise because Site 730 is located on the outer shoulder of an elevation (possibly a horst?), which would preclude significant lateral advection of fluids from the west.

Calcium and Magnesium

Concentrations of calcium generally increase linearly with depth at this site (Fig. 28), suggesting that distribution is controlled mainly by the upward diffusion of calcium from an unknown source below the base of the cored section. In contrast, the curvature in the magnesium profile between ~50 and ~250 mbsf (Fig. 28) indicates that dolomitization is occurring in this zone.

Ammonia, Phosphate, Silica, and Dissolved Organic Carbon

Ammonia concentrations are relatively low in Hole 730A, but they generally increase with depth even in the absence of sulfate reduction below ~225 mbsf (Fig. 28). Although methane content was not measured at this site, it is apparent that the increase in ammonia below ~200 m depth reflects production of NH_3 during methanogenesis. We suggest that because the organic matter in the upper ~110 m at Site 730 is old (and at best moderately preserved), it is likely to be nitrogen depleted. Such a depletion would explain the relatively low ammonia concentrations at depth.

As observed previously, phosphate concentrations are low throughout the hole, which is again attributed to the precipitation of small quantities of apatite (Fig. 28).

Maxima in the dissolved silica profile record two intervals, near 170 and 275 mbsf, where the sediments appear to be rela-

Table 5. Summary of interstitial water data, Site 730.

Core, sample interval (cm)	Depth (mbsf)	Vol. (mL)	pH	Alk. (mmol/L)	Sal. (g/kg)	Mg (mmol/L)	Ca (mmol/L)	Cl (mmol/L)	SO_4 (mmol/L)	PO_4 (μmol/L)	NH_4 (mmol/L)	SiO_2 (μmol/L)	Mg/Ca	DOC (a.u.)
117-730A-														
1H-4, 145-150	5.95		7.64	3.48	35.2	52.94	10.65	563	26.1	2.5	0.13	170	4.97	0.075
3H-4, 145-150	23.75	65	7.11	2.84	35.2	51.33	10.98	564	26.1	2.3	0.16	576	4.67	0.110
6X-4, 145-150	52.25	62	7.23	3.71	35.0	49.72	12.04	568	23.1	2.4	0.22	917	4.13	0.223
9X-4, 145-150	81.15	53	7.47	5.29	34.3	41.66	12.39	565	14.9	3.5	0.35	1065	3.36	0.532
12X-4, 145-150	110.15	41	7.40	6.33	33.6	35.89	12.28	566	7.6	2.5	0.74	1129	2.92	0.726
15X-4, 145-150	139.15	51	7.68	6.75	32.6	32.72	12.98	562	3.7	1.7	1.01	1097	2.52	0.793
18X-4, 145-150	168.15	46	7.45	5.34	32.6	30.29	13.11	564	2.2	1.6	1.22	1252	2.31	0.731
21X-4, 145-150	197.15	31	7.59	5.17	32.4	28.41	14.19	564	0.4	3.5	1.48	1103	2.00	0.680
24X-4, 145-150	226.15	25	7.61	4.34	32.4	28.26	14.58	564	0.4	3.2	1.60	1008	1.94	0.467
27X-2, 140-150	252.10	58	7.39	4.10	32.3	27.58	15.02	564	0	4.6	1.84	998	1.84	0.406
29X-4, 140-150	274.50	44	7.42	3.73	32.3	27.84	15.08	557	0	3.0	2.03	1141	1.85	0.340
33X-3, 140-150	331.60	30	7.42	3.27	32.2	28.07	15.41	564	0	2.0	2.29	850	1.82	0.305
37X-2, 140-150	348.80	30	7.16	3.12	32.2	26.99	16.81	567	0	1.0	2.64	800	1.61	0.292
39X-1, 140-150	366.60	25	7.15	2.76	32.2	26.93	16.79	569	0	1.0	2.88	733	1.60	0.223
42X-2, 140-150	397.10	35	7.48	1.92	32.2	26.68	17.04	566	0	0.7	2.49	669	1.57	0.236

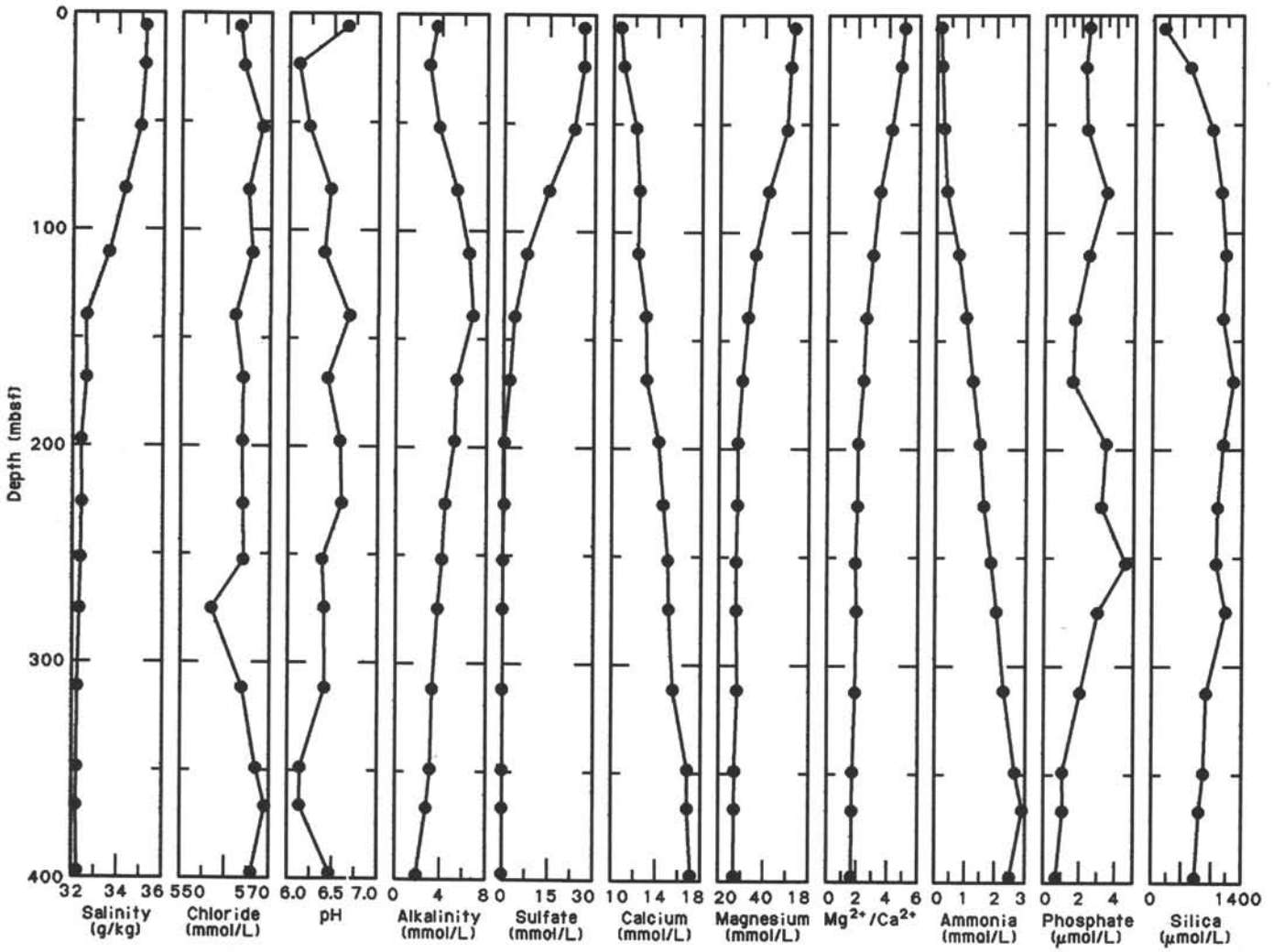

Figure 28. Concentration profiles vs. depth for Site 730.

tively enriched in opal (Fig. 28). The upper zone of enrichment is consistent with the observed abundance of siliceous microfossils in the hole (see "Biostratigraphy" section, this chapter). Radiolarian skeletons and diatom frustules are relatively rare in Core 117-730A-29X (~275 mbsf), but sponge spicules are common. This may account for the high dissolved silica concentration measured in the pore-water sample from that core. Biogenic silica is practically absent from the sediments below Core 117-730A-29X, which is reflected by the decreasing dissolved SiO_2 concentration below ~275 mbsf (Fig. 28).

Dissolved organic carbon (DOC) concentrations (Fig. 29) are lower at Site 730 than at the majority of Oman margin sites, which is consistent with the reduced level of diagenetic activity characteristic at this location. The DOC profile agrees only approximately with the organic carbon distribution (see "Organic Geochemistry" section, this chapter). Organic carbon concentrations range between 2% and 4% from ~40 to 110 mbsf. However, the absence of pronounced sulfate reduction, alkalinity, and metabolite production, and the rather low DOC in the pore waters of this zone suggests that the organic matter, even though abundant in places, may be relatively refractory when compared with other sites on the margin. This tentative conclusion is in agreement with the unusual history of sedimentation at this site, which has resulted in the presence of "old" organic matter in the near-surface strata.

ORGANIC GEOCHEMISTRY

Organic Matter Abundance and Character

We analyzed 44 samples, taken from all three lithologic units, for organic carbon and carbonate content (Table 2) and performed Rock-Eval pyrolysis on most of the above samples (Table 6).

Unit I consists of marly nannofossil ooze to a depth of 36.6 mbsf, and organic carbon values vary from 0.92% to 1.61%. The first 80 m of Unit II consist of marly nannofossil ooze and diatomaceous silty clays to a depth of 191 mbsf and are characterized by high organic carbon values that average 2.6%. The lower part of Unit II has distinctly lower values averaging 0.7% (Fig. 30 and Table 2). Unit III consists of foraminifer nannofossil chalks, and organic carbon values rarely exceed 0.5%.

The hydrogen (HI) and oxygen (OI) indices, plotted in a "van Krevelen-type" diagram (Fig. 31), cluster in an area which is characterized by somewhat lower HI when compared with samples from other margin sites. This might indicate that the organic matter is slightly more degraded at Site 730 than in comparison with Site 726.

Hydrocarbon Gases

Several unconformities, which could be effective seals for hydrocarbons, were visible on the seismic lines (see "Seismic Stra-

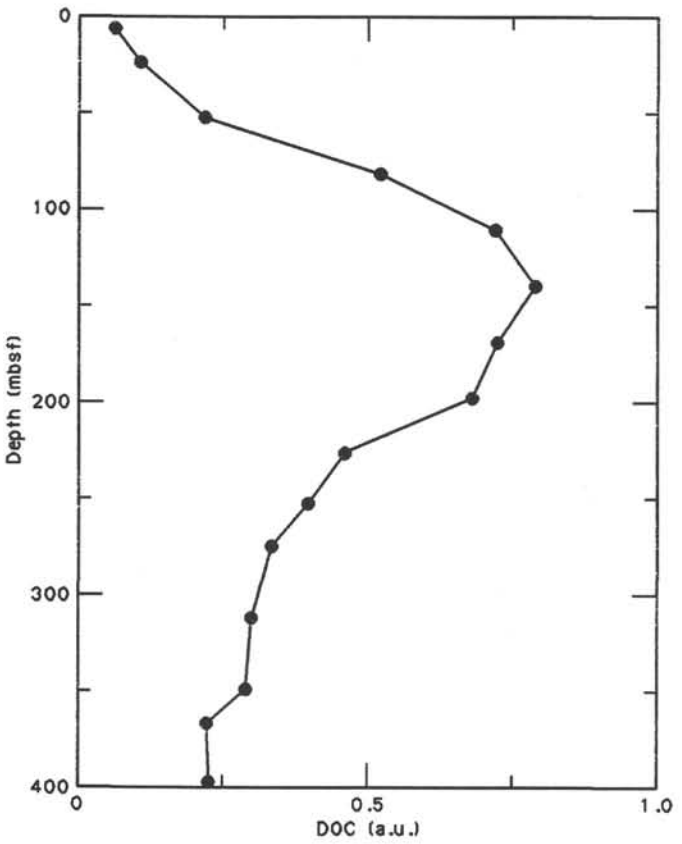

Figure 29. Profile of the relative concentration of dissolved organic carbon (DOC) at Site 730, plotted in absorbance units (a.u.).

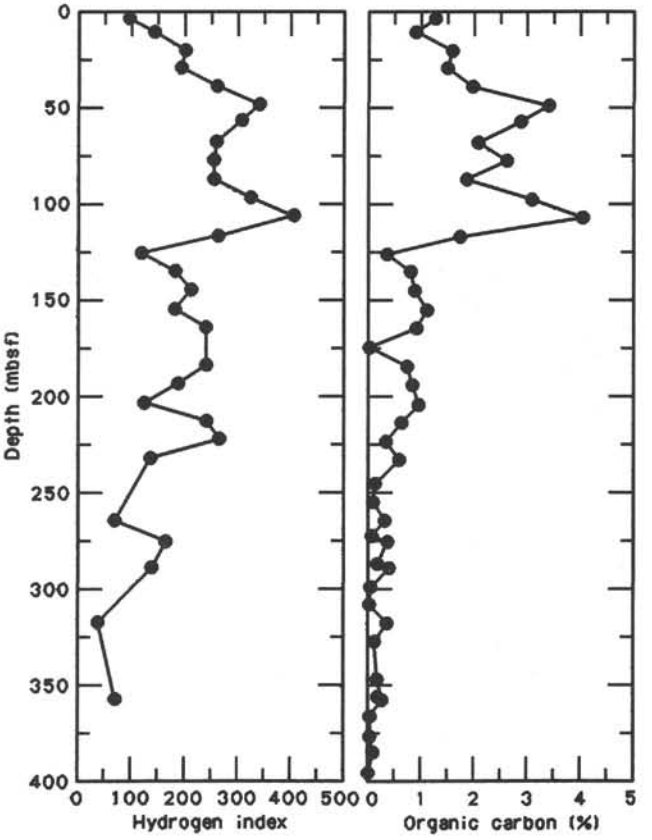

Figure 30. Downhole plot of organic carbon and hydrogen index values from pyrolysis for samples from Hole 730A.

Table 6. Results of Rock-Eval pyrolysis of sediment samples from Hole 730A.

Core, section interval (cm)	Depth (mbsf)	T_{max} (°C)	S_1	S_2	S_3	S_2/S_3	TOC	HI	OI
117-730A-									
1H-3, 78-80	3.78	424	0.21	1.24	1.77	0.70	1.28	96	138
2H-2, 78-80	10.58	426	0.18	1.33	1.35	0.98	0.92	144	146
3H-2, 130-132	20.60	424	0.37	3.23	1.80	1.79	1.61	200	111
4H-2, 78-80	29.58	420	0.33	2.95	3.63	0.81	1.51	195	240
5H-2, 80-82	39.10	416	0.74	5.22	4.22	1.23	1.99	262	212
6H-2, 105-107	48.90	415	1.57	11.63	2.78	4.18	3.39	343	82
7X-1, 130-132	57.00	411	2.03	8.92	2.19	4.07	2.88	309	76
8X-2, 109-111	68.09	418	0.85	5.46	2.28	2.39	2.09	261	109
9X-2, 78-80	77.48	417	0.91	6.74	2.05	3.28	2.63	256	77
10X-2, 78-80	87.18	419	0.69	4.85	2.32	2.09	1.88	257	123
11X-2, 110-112	97.20	413	1.88	10.14	3.92	2.58	3.10	327	126
12X-2, 78-80	106.48	418	2.27	16.39	3.58	4.57	4.04	405	88
13X-2, 128-130	116.68	416	0.70	4.68	4.53	1.03	1.76	265	257
14X-2, 78-80	125.78	417	0.12	0.46	1.69	0.27	0.38	121	444
15X-2, 30-32	135.00	417	0.29	1.51	1.93	0.78	0.82	184	235
16X-2, 14-16	144.54	416	0.36	1.93	1.48	1.30	0.91	212	162
17X-2, 73-75	154.83	421	0.30	2.12	1.78	1.19	1.15	184	154
18X-2, 36-38	164.06	419	0.27	2.25	1.91	1.17	0.93	241	205
20X-2, 93-95	184.03	417	0.28	1.86	1.60	1.16	0.77	241	207
21X-2, 78-80	193.48	414	0.31	1.63	1.40	1.16	0.86	189	162
22X-2, 123-125	203.63	414	0.25	1.24	1.40	0.88	0.98	126	142
23X-2, 88-90	212.98	417	0.27	1.56	1.68	0.92	0.64	243	262
24X-2, 71-73	222.41	417	0.17	0.93	1.47	0.63	0.35	265	420
25X-2, 87-89	232.27	412	0.20	0.84	1.58	0.53	0.61	137	259
28X-4, 80-82	264.20	408	0.05	0.23	1.04	0.22	0.32	71	325
29X-5, 70-72	275.30	410	0.13	0.61	1.50	0.40	0.37	164	405
31X-1, 87-89	288.77	409	0.15	0.57	1.88	0.30	0.41	139	458
34X-1, 50-52	317.40	422	0	0.15	0.47	0.31	0.37	40	127
38X-2, 21-23	357.31	410	0.03	0.19	1.24	0.15	0.27	70	459

Note: HI = hydrogen index and OI = oxygen index. For a detailed description of parameters, see "Explanatory Notes" chapter (this volume).

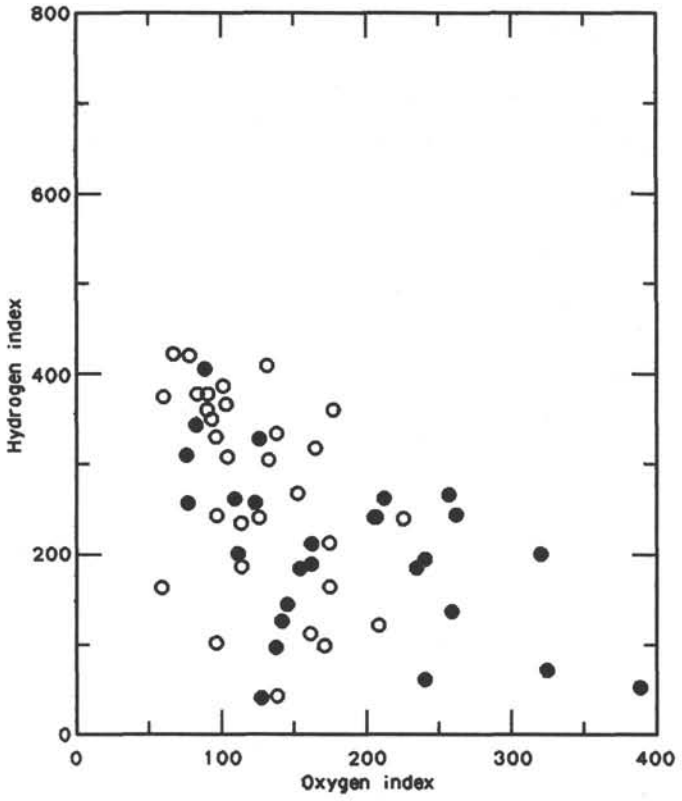

Figure 31. Plot of hydrogen index vs. oxygen index of samples from Hole 730A (dots), together with results from Hole 726A (circles).

tigraphy" section, this chapter), thereby warranting a careful monitoring of hydrocarbon gases during drilling. Gas pockets were virtually absent, however, and the only vacutainer sample collected from a suspected gas pocket (117-730A-17X-5, 145 cm) had a relatively low concentration of methane (28,481 ppm). Interstitial sulfate is depleted at a depth of 200 mbsf (see "Inorganic Geochemistry" section, this chapter), and the very low background values of organic carbon below this depth (average 0.25%) almost preclude the formation of biogenic methane.

INTERHOLE CORRELATIONS

Layer-by-Layer Correlation at Site 730

The one hole drilled at Site 730 is located in a water depth of 1066 m on the eastern flank of a midslope basement high that separates the slope basin into a shallow part and a deeper part. Hole 730A was drilled to 46.3 mbsf with the APC system and to 403.9 mbsf with the XCB. Recovery of APC-drilled cores was almost perfect in the hole, and the top of Hole 730A obtained the mud line. The age sedimentary sequence is mainly from middle to late Miocene age and is covered unconformably by late Pleistocene sediments.

We obtained detailed correlations in the upper 13 m of the covered sediments at Site 730. The upper interval has an age range from 0 to 0.3 Ma and is characterized by cyclic changes in the nature of sediments that can be identified by visual observation and by variations of magnetic susceptibility and $CaCO_3$ content.

Site-to-site correlations were made on the basis of visual identification of distinctive layers, as well as on physical and magnetic properties. Magnetic susceptibility was measured continuously and at 10-cm intervals before splitting the sections. Photographs were taken of the split cores.

Visual core correlations relied primarily on the core photographs. We were able to determine 26 distinct and traceable layers in the correlatable sedimentary sequence at Sites 723 and 724. These layers have been notated as OM-a_1,...h_4, and h_5, based on correlations between holes at Sites 723 and 724 (see "Lithostratigraphy" sections, "Site 723" and "Site 724" chapters, this volume). The letter code (i.e., a, b, c, etc.) refers to the sequence of cores, and the number code indicates the number of marker layers in each core. For example, the notation "a_2" corresponds to the second marker layer defined in Core 117-723A-1H, and "b_1" denotes the first marker layer in Core 117-723A-2H. Marker layers a_1–h_4 were defined on the cored sediments of Hole 723A. Three marker layers (c_5, e_3, and h_5) were defined on the sedimentary sequence at Hole 724A in addition to those noted at Site 723.

Criteria for defining a marker layer are (1) the layer is distinct enough to trace in the sedimentary sequence of the other holes and (2) the character of the layer does not change. Useful criteria for recognizing a marker layer include color boundaries, distinctly colored layers, shape of bioturbations, and sequences of color change in surrounding sediments. We have traced the same marker layers from Sites 723 and 724 to Sites 727 and 728. At Site 730, the upper 16 marker layers are traced. Table 7 lists the depth of the traced marker layers in the Oman margin sites (i.e., Sites 723, 724, 727, 728, and 730).

Figure 32 shows the magnetic susceptibility curve and the positions of individual, visually correlatable layers. The pattern of the magnetic susceptibility and the positions of the layers match very well between Sites 728 and 730. The stratigraphy of the magnetic susceptibility data and the visually identified layers are extremely consistent in that a particular visually characteristic layer always coincides in depth with a distinct feature in the magnetic susceptibility curve. Since stratigraphic control in the top of Site 730 is poor, these site-to-site correlations should prove useful in future studies on the Pleistocene section of Site 730.

SUMMARY AND CONCLUSIONS

Site 730 is the last site drilled on the Oman continental margin and was added to the operations schedule after Site 729 was abandoned due to poor hole conditions. Similar to Sites 723 and 727, the site is located near the bottom of the pronounced OMZ that impinges on the margin. Site 730 is positioned to the east of a ridge that is presumably ophiolitic basement and that separates the upper and lower sedimentary basins. Sediments of the upper basin, which were previously drilled only 6 km to the west at Site 727, onlap eastward onto the ridge and are thinned and tilted by tectonic movement of the ridge. East of the basement ridge, seismic reflection profiles reveal a prominent unconformity that truncates eastward-dipping beds.

We moved upsection on the eastward-dipping reflectors and cored through the unconformity to recover older strata at Site 730 than those previously cored at Site 727. The age of sediments and hiatuses, and the evolution of the sediment facies, were expected to be useful in reconstructing the subsidence, as well as the erosional and tectonic history, of the slope basins and the prominent basement ridges.

Some of the major findings at Site 730 are summarized in Figure 33 and include the identification of

1. a significant hiatus ranging in age from Pleistocene to upper Miocene;
2. the occurrence of siliceous sediments in the middle and late Miocene that appear earlier here but are generally equivalent to the siliceous facies recovered on the Owen Ridge;
3. the appearance of *Globerigina bulloides,* an upwelling indicator, in the lower middle Miocene, which is earlier than its appearance on the Owen Ridge; and

Table 7. List of stratigraphic depth marker layers at Sites 723, 724, 727, 728, and ODP depth of marker layers at Site 730.

	Hole 723B		Hole 724A		Holes 727A and B		Holes 728A and B		Hole 730A	
Layer	Core, section, interval (cm)	Corrected depth (mbsf)	Core, section, interval (cm)	Corrected depth (mbsf)	Core, section, interval (cm)	Corrected depth (mbsf)	Core, section, interval (cm)	Corrected depth (mbsf)	Core, section, interval (cm)	ODP depth (mbsf)
OM-a_1	1H-3, 35	3.35	1H-1, 95	0.95	1H-2, 15	1.65	1H-1, 65	0.65		
a_2	2H-3, 20	7.20	1H-2, 115	2.65	1H-3, 55	3.55	1H-1, 135	1.75	1H-1, 120	1.20
b_1	2H-4, 65	9.15	1H-3, 100	4.00	1H-3, 15	6.55	1H-2, 90	2.80	1H-2, 85	2.35
b_2	2H-6, 110	12.60			1H-4, 90	8.80	1H-3, 110	4.50	1H-3, 115	4.15
b_3	3H-1, 95	14.75	2H-1, 75	7.95	1H-5, 80	10.20	1H-4, 40	5.30	1H-4, 55	5.05
c_1	3H-5, 110	20.90	2H-2, 75	9.45	2H-1, 50	14.00	1H-5, 70	7.10	1H-5, 25	6.25
c_2	4H-1, 85	24.95	2H-3, 130	11.50	2H-2, 125	16.25	1H-6, 50	8.40	1H-5, 110	7.10
c_3	4H-2, 100	26.60	2H-4, 70	12.40	2H-3, 95	17.45	1H-6, 115	9.05	1H-6, 10	7.60
c_4	4H-3, 15	27.25	2H-4, 120	12.90	2H-4, 30	18.30	1H-7, 40	9.80	2H-1, 35	8.65
c_5	4H-3, 100	28.10	2H-5, 35	13.55	2H-4, 55	18.55	2H-1, 35	10.45		
d_1	4H-5, 70	30.80	3H-1, 40	17.20	2H-5, 100	20.50	2H-2, 5	11.65	2H-2, 45	10.25
d_2	4H-6, 10	31.70	3H-1, 150	18.30	2H-6, 15	21.15	2H-2, 25	11.85	2H-2, 65	10.45
d_3	4H-7, 5	33.15	3H-2, 90	19.20	2H-6, 110	22.10	2H-2, 50	12.10	2H-2, 95	10.75
d_4	5H-2, 50	35.30	3H-3, 85	20.65	3H-1, 90	23.90			2H-2, 130	11.10
e_1	5H-5, 20	39.50	3H-4, 15	21.45	3H-3, 5	26.05	2H-2, 95	12.55	2H-3, 55	11.85
e_2	6H-1, 90	43.80	3H-5, 90	23.70	3H-5, 25	29.25	2H-2, 140	13.00	2H-3, 115	12.45
e_3	6H-3, 150	47.40	3H-6, 95	25.25	3H-5, 130	30.30	2H-3, 60	13.70	2H-4, 40	13.20
f_1	6H-5, 120	50.10	4H-1, 85	27.75	3H-7, 25	32.25	2H-4, 20	14.80		
f_2	7H-2, 15	54.25	4H-2, 70	29.10	4H-2, 95	34.95	2H-4, 55	15.15		
g_1	7H-6, 30	60.40	4H-4, 120	32.60	4H-4, 100	38.00	2H-5, 35	16.45		
g_2	8H-2, 60	64.40	4H-6, 25	34.65	4H-7, 40	41.90	2H-5, 105	17.15		
h_1	8H-5, 90	69.20	4H-7, 40	36.30	5H-4, 40	46.80	2H-6, 70	18.30		
h_2	9H-1, 20	72.10	5H-1, 80	37.30			2H-7, 35	19.45		
h_3	9H-3, 135	76.25	5H-2, 60	38.60	5H-6, 135	50.75	3H-1, 90	20.70		
h_4	9H-7, 95	81.85	5H-4, 145	42.45	6H-3, 95	55.35	3H-2, 65	21.95		
h_5			5H-5, 145	43.95	6H-4, 95	56.85	3H-2, 150	22.80		

Note: Corrected depth = corrected depth for stratigraphic thickness.

4. the presence of slumps, faults, and turbidites in the middle Miocene that indicate tectonic instability of the marginal slope basins.

The sediments at Site 730 range from Holocene to late early Miocene age and have been divided into three lithologic units. Unit I consists of marly nannofossil ooze to a sub-bottom depth of 15.2 mbsf. No siliceous fossils occur in this unit. A major hiatus spanning nannofossil Zones NN21–NN10 was found in Core 117-730A-2H; it separates lithologically similar sediments of Pleistocene and late Miocene age (Fig. 33). The rate of sedimentation in the interval above the hiatus was established as 44 m/m.y.

Unit II comprises marly nannofossil oozes and diatomaceous silty clays, which are late and middle Miocene age, and extends downsection to 201 mbsf. Diatom frustules and radiolaria are abundant from 33 to 150 mbsf, where they begin to decrease in abundance and completely disappear by the early middle Miocene (about 280 mbsf).

Foraminifer nannofossil chalks dominate Unit III, which extends downsection to about 404 mbsf. Unit III is late early Miocene (NN4) age (Fig. 33). Such structural features as slump beds 10–200 cm thick, recumbent folds, and high-angle faults that offset bioturbation traces and color laminations characterize this unit. Turbidites that contain shallow-water material are commonly associated with the slump structures in the middle of Unit III, but they are rare at the base of Unit III. Throughout the recovered section, the occurrence of siliceous microfossils coincides with poor preservation of planktonic and benthic foraminifers, which are progressively recrystallized with depth.

The chemical compositions of interstitial waters show no indication of a sub-bottom supply of sulfate, and diagenetic reactions appear to be dominated by carbonate cementation and methanogenesis (Fig. 33). High values of organic carbon (2%–3%) occur only in the upper part of Unit II (upper Miocene) and are distinctly lower (<1%) throughout the remaining section (Fig. 33).

Site 730 provided several types of new information about the Oman margin. First, it showed that opal deposition and upwelling began earlier on the Oman margin than it did on the offshore Owen Ridge. Second, it provided information about the tectonic stability and uplift history of the slope basins and their associated basement ridges.

REFERENCES

Bathurst, R.G.C., 1975. *Carbonate sediments and their diagenesis.* Developments in Sedimentary (Vol. 12): New York-London-Amsterdam (Elsevier).

Berggren, W. A., Kent, D. V., and Van Couvering, J. A., 1985. The Neogene: Part 2, Neogene chronology and chronostratigraphy. *In* Snelling, N. J. (Ed.), *The Chronology of the Geological Record*: Geol. Soc. Mem. (London), 10:211–260.

Bukry, D., 1973. Low-latitude coccolith biostratigraphic zonation. *In* Edgar, N. T., Saunders, J. B., et al., *Init. Repts. DSDP*, 15: Washington (U.S. Govt. Printing Office), 685–703.

_____, 1975. Coccolith and silicoflagellate stratigraphy, northwestern Pacific Ocean, Deep Sea Drilling Project Leg 32. *In* Larson, R. L., Moberly, R., et al., *Init. Repts. DSDP*, 32: Washington (U.S. Govt. Printing Office), 677–701.

Hamilton, E. L., 1978. Sound velocity-density relations in sea-floor sediments and rocks. *J. Acoustic. Soc. Am.*, 63:366–377.

Johnson, D. A., and Nigrini, C. A., 1985. Synchronous and time-transgressive Neogene radiolarian datum levels in the equatorial Indian and Pacific Oceans. *Mar. Micropaleontol.*, 9:489–523.

Takayama, T., and Sato, T., 1987. Coccolith biostratigraphy of the North Atlantic Ocean, Deep Sea Drilling Project Leg 94. *In* Ruddiman, W. F., Kidd, R. B., et al., *Init. Repts. DSDP*, 94, Pt. 2: Washington (U.S. Govt. Printing Office), 651–702.

Ms 117A-117

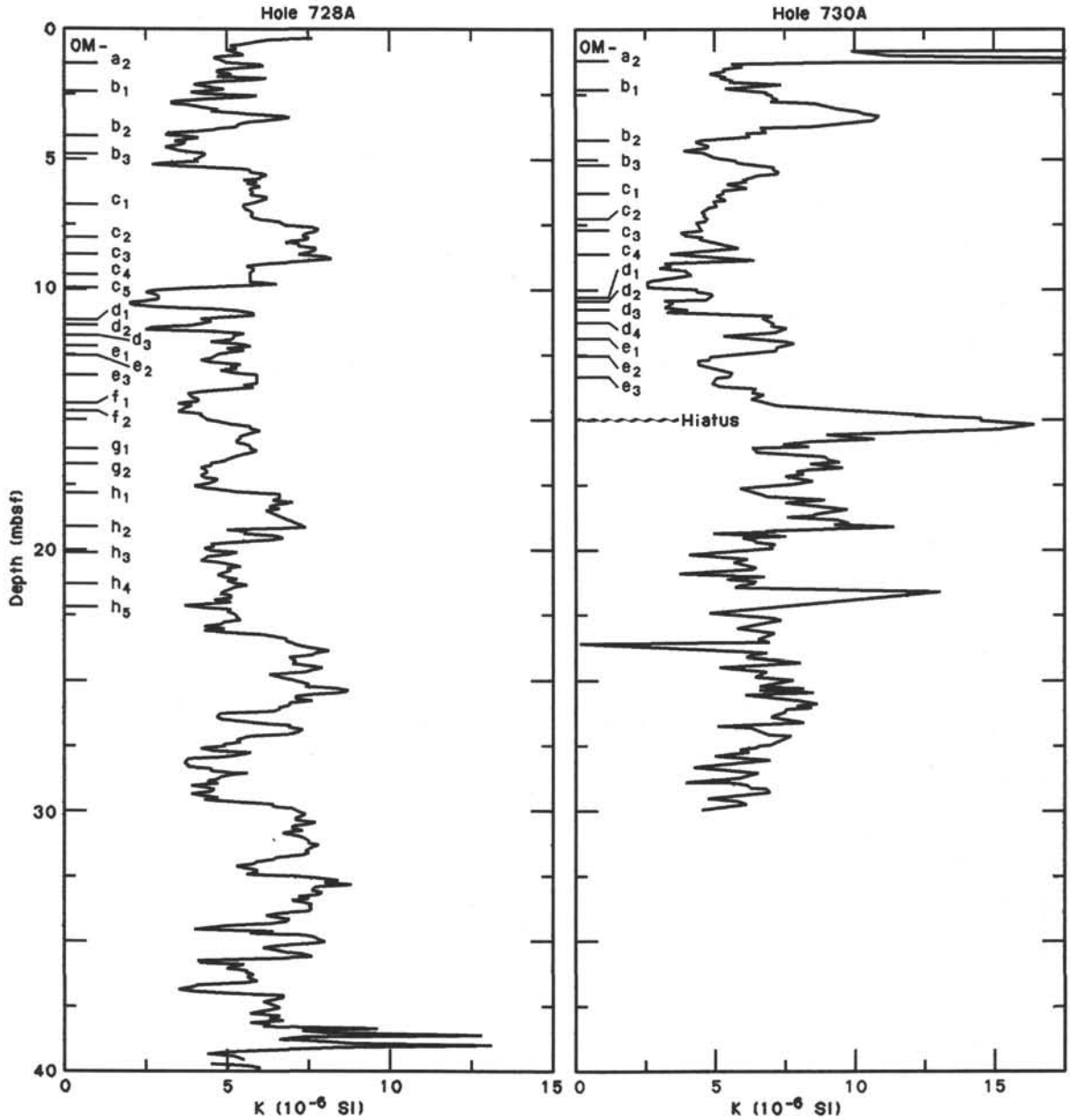

Figure 32. Volume magnetic susceptibility curve and positions of the marker layers in Holes 728A and 730A.

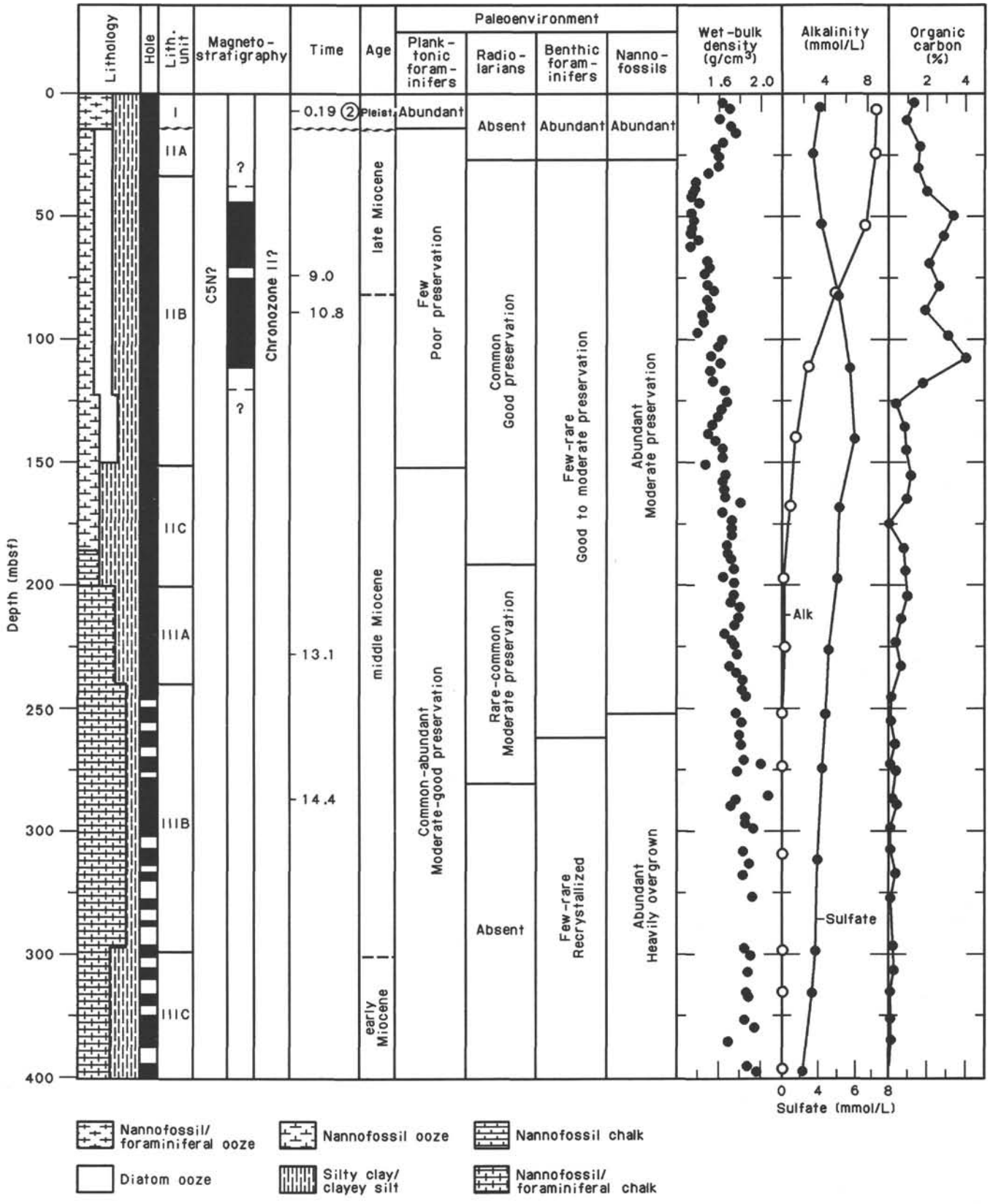

Figure 33. Summary chart outlining preliminary shipboard findings at Site 730.